



## Processes Controlling Methane Emissions From a Tropical Peatland Drainage Canal

Lauren Somers, Alison Hoyt, Alexander Cobb, Suhailah Isnin, Muhammad Asri Akmal Bin Haji Suhip, L. Gandois, Rahayu Sukri, Charles Harvey

### ► To cite this version:

Lauren Somers, Alison Hoyt, Alexander Cobb, Suhailah Isnin, Muhammad Asri Akmal Bin Haji Suhip, et al.. Processes Controlling Methane Emissions From a Tropical Peatland Drainage Canal. Journal of Geophysical Research: Biogeosciences, 2023, 128 (3), 10.1029/2022JG007194 . hal-04050057

**HAL Id: hal-04050057**

**<https://hal.science/hal-04050057>**

Submitted on 31 Mar 2023

**HAL** is a multi-disciplinary open access archive for the deposit and dissemination of scientific research documents, whether they are published or not. The documents may come from teaching and research institutions in France or abroad, or from public or private research centers.

L'archive ouverte pluridisciplinaire **HAL**, est destinée au dépôt et à la diffusion de documents scientifiques de niveau recherche, publiés ou non, émanant des établissements d'enseignement et de recherche français ou étrangers, des laboratoires publics ou privés.



Distributed under a Creative Commons Attribution 4.0 International License

# JGR Biogeosciences



## RESEARCH ARTICLE

10.1029/2022JG007194

### Key Points:

- Methane emissions increase over the first kilometer of a canal, before leveling off, even as methane concentrations decrease downstream
- Canals may be substantial contributors to both methane and carbon dioxide emissions of disturbed tropical peatlands
- Under low to moderate flow conditions, 70% of methane advected into a drainage canal was oxidized and 26% was emitted to the atmosphere

### Supporting Information:

Supporting Information may be found in the online version of this article.

### Correspondence to:

L. D. Somers,  
[Lauren.Somers@Dal.ca](mailto:Lauren.Somers@Dal.ca)




### Citation:

Somers, L. D., Hoyt, A., Cobb, A. R., Isnin, S., Suhip, M. A. A. b. H., Sukri, R. S., et al. (2023). Processes controlling methane emissions from a tropical peatland drainage canal. *Journal of Geophysical Research: Biogeosciences*, 128, e2022JG007194. <https://doi.org/10.1029/2022JG007194>

Received 16 SEP 2022

Accepted 25 JAN 2023

## Processes Controlling Methane Emissions From a Tropical Peatland Drainage Canal

Lauren D. Somers<sup>1,2</sup> , Alison Hoyt<sup>3</sup>, Alexander R. Cobb<sup>4</sup> , Suhailah Isnin<sup>4</sup>, Muhammad Asri Akmal bin Haji Suhip<sup>5</sup>, Rahayu S. Sukri<sup>5</sup> , Laure Gandois<sup>6</sup>, and Charles Harvey<sup>2,4</sup>

<sup>1</sup>Civil and Resource Engineering, Dalhousie University, Halifax, NS, Canada, <sup>2</sup>Civil and Environmental Engineering, Massachusetts Institute of Technology, Cambridge, MA, USA, <sup>3</sup>Earth System Science, Stanford University, Stanford, CA, USA, <sup>4</sup>Singapore-MIT Alliance for Research and Technology, Singapore, Singapore, <sup>5</sup>Institute for Biodiversity and Environmental Research, Universiti Brunei Darussalam, Jalan Tungku Link, Brunei Darussalam, <sup>6</sup>Laboratoire Ecologie Fonctionnelle et Environnement, Université de Toulouse, CNRS, INPT, UPS, Toulouse, France

**Abstract** Most peat domes in Southeast Asia are crisscrossed by networks of drainage canals. These canals are a potentially important source of methane to the atmosphere because the groundwater that discharges into them carries high concentrations of dissolved methane that is produced within peat. In this study, we present an isotope-enabled numerical model that simulates transport, degassing, and oxidation of methane and dissolved inorganic carbon (DIC) along a drainage canal. We then estimate methane fluxes through a 5-km canal that crosses a disturbed, forested, but undeveloped, peat dome in Brunei Darussalam by applying this model to field data: concentrations and stable carbon isotopic ratios of both methane and dissolved inorganic carbon from both peat porewater and canal water. We estimate that approximately 70% of the methane entering the canal is oxidized within the canal, 26% is degassed to the atmosphere, and 4% is transported toward the ocean, under low to moderate flow conditions. The flux of methane to the atmosphere is lowest at the maximum elevation of the canal, where flow is stagnant and methane concentrations are highest. Downstream, as flow velocity increases, methane emissions plateau even as methane concentrations decrease. The resulting methane emissions from the canal are large compared to emissions from the peat surface and vegetation on a per-area basis. However, since the canal covers only a small portion of the catchment area, the canal may be a substantial but not dominant source of methane from the peatland.

**Plain Language Summary** Peatlands in Southeast Asia store large amounts of organic carbon as waterlogged, partially decayed plant matter (peat). Over recent decades, half of the region's peatlands have been drained for conversion to agricultural and forestry plantations using canal networks. This drainage lets oxygen enter the peat, enabling microbes to breakdown the peat, drastically increasing the amount of carbon dioxide emitted to the atmosphere. However, the impacts of drainage on methane, another important greenhouse gas, are poorly understood. In this study, we use the naturally occurring variation in the weight of carbon atoms (carbon isotopes) to track microbial methane consumption and emission to the atmosphere in drainage canals. We created a mathematical model that uses the carbon isotope data to track what happens to methane in a drainage canal. We determined that a large amount of methane is transported with shallow groundwater flow into the drainage canals and that most of the methane that flows into drainage canals is consumed by microbes in the canal. The remaining methane is emitted to the atmosphere, making drainage canals an important but not dominant contributor to the overall methane budget of a disturbed tropical peatland.

## 1. Introduction

Tropical peatlands in Southeast (SE) Asia have suffered large-scale disruption in recent decades, jeopardizing a globally important carbon store (Hooijer et al., 2012; Page et al., 2011; Warren et al., 2017). In 2015, only 29% of Southeast Asian peatlands remained forested compared to 76% in 1990. Most of the deforested area has been converted to managed landcover which includes small-holder areas and industrial plantations (oil palm and pulp plantations), where drainage canals lower the water table (Miettinen et al., 2016). Recent satellite mapping by Dadap et al. (2021) shows that drainage canals are present in 65% of Southeast Asian peatlands. Drainage allows oxygen into previously anoxic peat, accelerating oxidation of organic matter, dramatically increasing carbon dioxide emissions, land subsidence, and fire risk (Dadap et al., 2019; Field et al., 2009; Hirano et al., 2007;

© 2023. The Authors.

This is an open access article under the terms of the [Creative Commons Attribution License](https://creativecommons.org/licenses/by/4.0/), which permits use, distribution and reproduction in any medium, provided the original work is properly cited.

Hooijer et al., 2010, 2012; Hoyt et al., 2020; Miettinen et al., 2017; Page et al., 2009). Against this backdrop of rapid peatland transformation, methane emissions in disturbed tropical peatlands remain poorly understood.

Throughout tropical peatlands, microbes generate methane below the water table where the consistently warm, saturated, and anoxic conditions are ideal for methanogenesis (Limpens et al., 2008). Methane generated in tropical peatlands can escape through several pathways: (a) Diffusion of methane from the peat surface has been widely described in the literature (e.g., Deshmukh et al., 2020; Hirano et al., 2009; Melling et al., 2005). This flux is typically small relative to temperate and northern peatlands and is often negative, indicating a slight uptake of methane by the surface peat (Couwenberg et al., 2010). (b) Ebullition can carry methane to the peat surface producing large and sporadic surface fluxes, if dissolved gas concentrations are sufficiently high (Teh et al., 2017). (c) Methane is emitted from the stems and trunks of plants and trees, particularly where roots channel methane through internal air spaces (Pangala et al., 2013; Sjögersten et al., 2020). (d) Finally, methane dissolved in porewater is transported with groundwater flow to discharge in surface water bodies (Bange et al., 2019; Hoyt, 2017). A recent study from Brunei showed that advection in flowing groundwater accounts for a larger proportion (65%) of tropical peatland methane production than previously thought, explaining the lower surface fluxes compared to northern and temperate peatlands (Hoyt, 2017).

The effect of drainage on net methane emissions, accounting for all four of these fluxes across a peat dome, remains unclear. On one hand, drainage decreases total methane production by lowering the water table so that oxygen enters the shallow peat (Hirano et al., 2009). Accordingly, several recent studies showed lower methane surface fluxes from drained peatlands relative to intact peat swamp forest in Southeast Asia (e.g., Adji et al., 2014; Deshmukh et al., 2020; Hirano et al., 2009; Ishikura et al., 2018; Wong et al., 2020). On the other hand, streams and rivers can be significant contributors to aquatic methane emissions (Bange et al., 2019; Crawford et al., 2014) and drainage canals may create new sources of degassing to the atmosphere. Given that most tropical peatlands in Southeast Asia are drained (Dadap et al., 2021), drainage canals could be an important pathway for greenhouse gas emissions.

This paper focuses on the fate of methane that is advected laterally through peat (pathway d above) and discharged into man-made drainage canals. Some drainage canals, like our study canal, cross peat domes, draining to either side of a flow divide (Figure 1a). Other drainage canals originate in the dome and only flow in one direction. In either case, turbulent mixing, and hence atmospheric gas exchange, increases downstream as the canal captures more discharge, the gradient steepens, and flow accelerates. Turbulent mixing works to both increase methane degassing and increase methane oxidation by mixing more oxygen into the canal. The net result of such competing processes can be ascertained by constructing a mass-balance model that formulates the competing processes and collecting field data to parameterize these processes.

The few existing studies of methane emissions from drainage canals use floating gas flux chambers to measure methane fluxes (Jauhiainen & Silvennoinen, 2012; Kent, 2019; Manning et al., 2019). The observed fluxes are highly variable but orders of magnitude higher than fluxes from the surface of surrounding peatlands, suggesting that drainage canals may be hotspots for methane outgassing. These floating chamber measurements are subject to large spatial variability, with individual measurements ranging from non-detectable to  $50,780 \text{ g CH}_4 \text{ ha}^{-1} \text{ d}^{-1}$  (Jauhiainen & Silvennoinen, 2012). Also, chamber methods alone do not provide insight into the flux of methane entering drainage canals or the rate of oxidation of methane within canals by methanotrophic microbes.

We require new methods to assess the magnitude and mechanisms of methane emissions from drainage canals. Stable carbon isotopes can serve as a useful tool to monitor methane dynamics in peatlands (Holmes et al., 2015; Hoyt, 2017; Sancı & Panarello, 2015) and can be applied to drainage canals. Carbon isotopes can be used to help distinguish between methane oxidation and degassing. Microbial oxidation of methane causes isotopic fractionation because the reaction rate for  $^{12}\text{CH}_4$  is faster than for  $^{13}\text{CH}_4$ , altering the  $\delta^{13}\text{C}$  of both the  $\text{CH}_4$  and  $\text{CO}_2$  dissolved in the canal water. Degassing, on the other hand, does not cause substantial fractionation of  $\text{CH}_4$  and  $\text{CO}_2$ .

Combining a carbon mass-balance model with measurements of solute concentrations and carbon isotopes in canal water has the potential to provide better estimates of total emissions along the canal than chamber measurements. First, this approach integrates upstream processes, avoiding the problems caused by extreme variability in floating chamber measurements. Second, this method takes advantage of different measurements,  $\text{CH}_4$  and  $\text{CO}_2$  and their isotopes, that contain different but complimentary information.

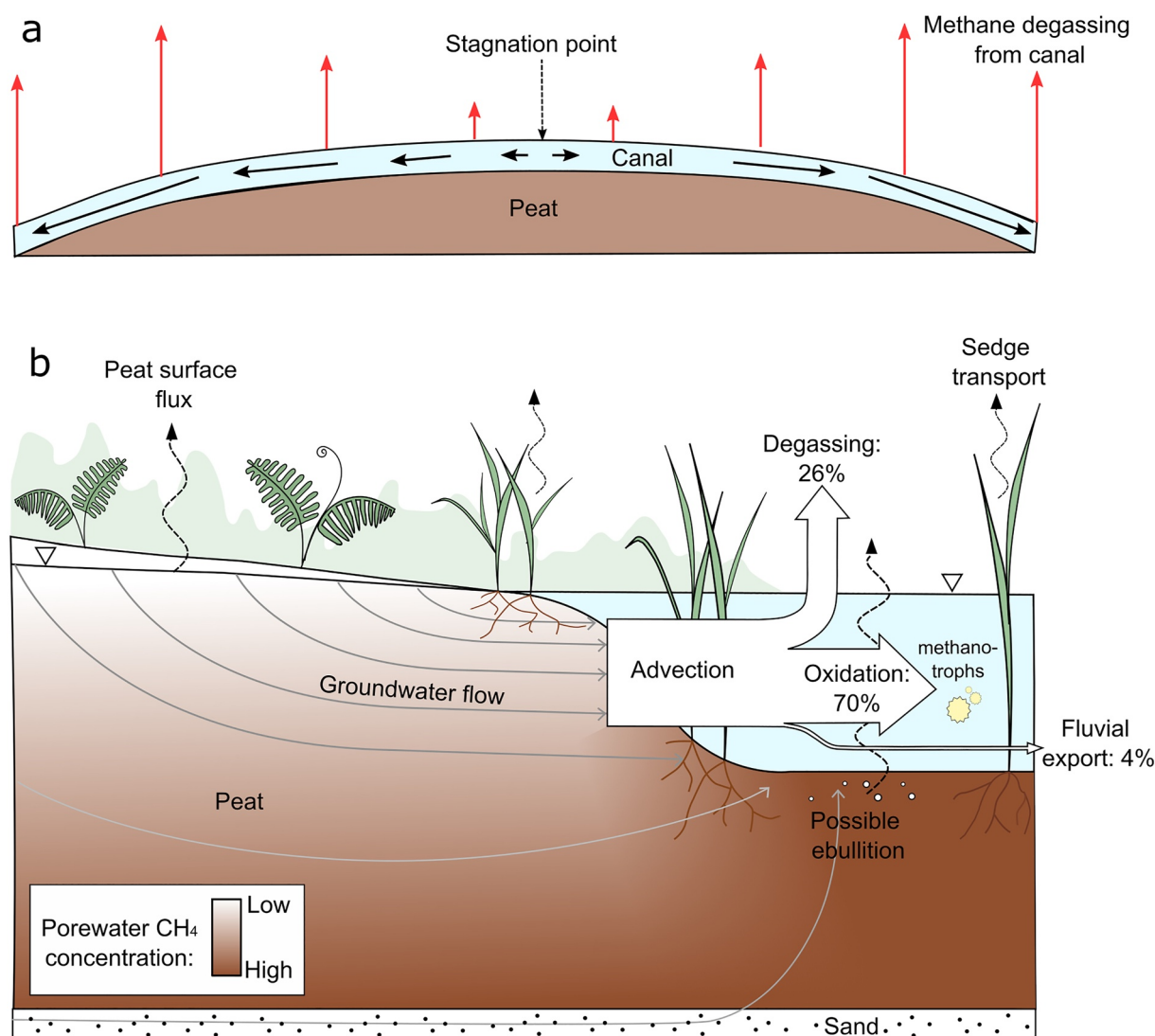


**Figure 1.** Conceptual model of methane dynamics in a tropical peatland canal based on previous work (e.g., Akhtar et al., 2020; Bange et al., 2019; Hoyt, 2017) and the present study. (a) Cross section along canal illustrating the canal flow divide and increasing methane emissions further downstream. (b) Cross section perpendicular to canal illustrating the fate of methane advected into the drainage canal.

In this paper, we formulate methane fluxes and isotopic fractionation processes in a model of flow and advection that accounts for increases in gas exchange with flow velocity along the canal. We aim to: (a) create a reactive-transport model of the carbon isotope dynamics as methane and DIC enter and move through the canal and; (b) determine the amounts of methane that are transported into a canal with groundwater, oxidized in the canal and emitted to the atmosphere at the canal surface, under differing flow conditions.

## 2. Materials and Methods

Our approach combines stable carbon isotopic measurements with hydrologic monitoring and modeling, as described in the coming sections. Briefly, we collected porewater and canal water samples along the Badas Canal in Brunei Darussalam. These samples were analyzed for concentration and  $\delta^{13}\text{C}$  of  $\text{CH}_4$  and  $\text{CO}_2$ , and major ions during two different flow conditions. We also monitored streamflow at the canal outlet and water table elevation in the peatland. We developed an isotope-enabled reactive transport model for  $\text{CH}_4$  and  $\text{CO}_2$  along the length of the canal and fit it to our observed data. The fitted model is used to quantify the total amounts of methane entering the canal from porewater inflow (advection through the peat), methane oxidation in the canal, degassing from the



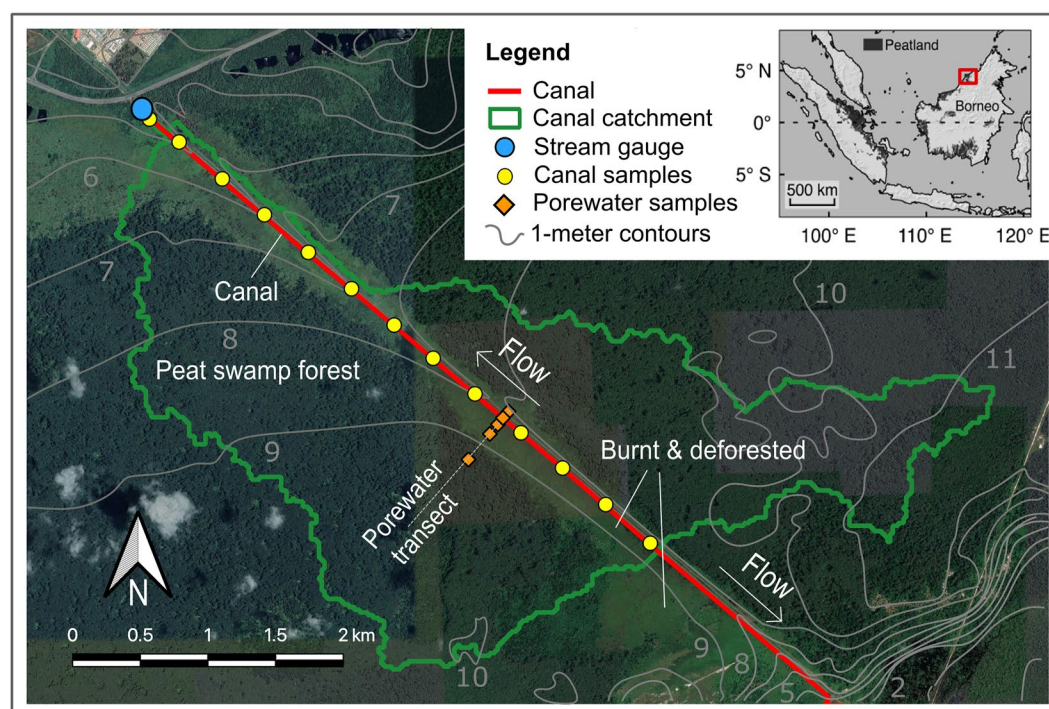


**Figure 2.** Site map showing the study site location in Brunei, Borneo (inset) and Badas peat dome including the canal, canal catchment area (for flow to the northwest) and sampling locations.

canal water surface, and canal outflow. Fitted model parameters provide insight into spatial and temporal controls on methane emissions.

## 2.1. Study Site

The Badas peat dome is located in the Belait district of Brunei Darussalam on the island of Borneo (4°35'N, 114°23'E; Figure 2). In the late 1960s or early 1970s a drainage canal was excavated across the peat dome to prevent flooding on the Badas Road, a service road that facilitates maintenance of a water pipeline from the Belait River to oil and gas operations on the coast. The drainage canal lowered the water table and dried out the surrounding surface peat such that fires destroyed some of the peat swamp forest adjacent to the canal (Suhip et al., 2020). In 2014, Brunei Shell Petroleum Co Sdn Bhd and Wetlands International constructed a series of canal blocks consisting of compressed peat to limit drainage.

We focus on a five-km section of the Badas Canal that extends from a natural topographic divide (where water flows are in opposite directions on either side of a stagnation point) to a downstream outflow at the northwestern end of the canal where we monitor canal discharge. The average canal width is approximately 10 m with some random variation. The canal is 1–2.5 m deep at its deepest point in the cross section. The canal has an average slope of approximately 0.0007. The slope increases gradually in the downstream direction with no notable steps or riffles. The study section of the canal drains an area of 10.66 km<sup>2</sup>. The canal water temperature ranges from approximately 26° to 30°C.

About 84% of the catchment area is covered by intact peat swamp forest dominated by *Shorea albida*, a 50 m tall species of dipterocarp tree. The burnt and deforested portion of the catchment (~16%) is covered with ferns (*Nephrolepis* sp.) and sedges (*Scleria sumatrensis*), with sedges mainly located near the canal (nearby study areas further described by Akhtar et al., 2020; Dommain et al., 2015; Gandois et al., 2013; and Hoyt et al., 2019). Beneath the land surface, we observed peat deposits up to around 7 m thick and underlain by fine white sand. Average annual rainfall from 1947 to 2004 was 2.88 m/year in the nearby towns of Seria and Kuala Belait. Precipitation does not exhibit strong seasonality but September to January are typically the wettest months.

## 2.2. Water Sampling

### 2.2.1. DIC, Methane, and $\delta^{13}\text{C}$

We collected porewater and canal water samples during two field campaigns for analysis of concentration and  $\delta^{13}\text{C}$  of  $\text{CH}_4$  and dissolved inorganic carbon (DIC) in January and August 2020. In January 2020, samples were also analyzed for  $\delta^2\text{H}$  of  $\text{CH}_4$ . Given the low pH of the porewater and canal water at nearby sites ( $\sim 3.5\text{--}4.5$ ; Gandois et al., 2013), DIC is predominantly present as  $\text{CO}_2$  and the two can be considered equivalent. In January 2020, our six porewater sampling sites were arranged in a transect perpendicular to the canal at distances of 30, 60, 150, 370 m west of the canal (PT1-30W to PT1-370W), 60 m east of the canal (PT1-60E) and one profile directly through the canal and the underlying peat (PT1-D1). At each site, 13–15 water samples were collected in a vertical profile from 0.3 m below the peat surface (0.1 m below water surface for the canal vertical profile) to the bottom of the peat layer. Porewater samples were collected with Pushpoint and Sedpoint piezometers (see Gandois et al., 2013 for additional detail; MHE Designs) and a peristaltic pump. In August 2020, porewater samples were collected only at PT1-30W. We also cored the peat at three transect locations: 60, 150 and 370 m west of the canal using a Russian corer to determine the depth of the peat and composition of the underlying sediment.

Canal water samples were collected approximately every 400 m along the canal from the upstream flow divide to the canal outlet, where the stream passes through a culvert under the Seria bypass highway, 5,070 m downstream. In January 2020, samples were collected at a single depth of 0.3 m below the water surface. In August 2020, samples were collected at depths of 0.3 m below the water surface and 0.3 m above the canal bed. Samples were collected approximately 1–2 m horizontally from the eastern bank of the canal.

All water samples for  $\text{CO}_2$ ,  $\text{CH}_4$ , and isotopes were collected in 12 mL glass Exetainer™ vials (Labco Ltd.).  $\text{CH}_4$  samples were field acidified to a pH of less than 2 using HCl. No preservatives were added to the DIC measurements for the January 2020 field campaign. During the August 2020 field campaign, DIC samples were poisoned with  $\text{ZnCl}_2$  to preserve them under possible shipping delays caused by the COVID-19 pandemic. All samples were refrigerated at 4°C before being express shipped on ice within 2 weeks of collection to the Stable Isotope Facility at UC Davis, California for analysis.

### 2.2.2. Major Ions

We collected 30 mL water samples in plastic bottles in January 2020 at the same locations as DIC and  $\text{CH}_4$  sampling, to be analyzed for major ion concentrations. These samples were filtered through 0.2  $\mu\text{m}$  filters and stored at 4°C for 6 months before being analyzed for fluoride, chloride, bromide, sulfate, phosphate, sodium, potassium, magnesium, and calcium ions by ion chromatography at the Functional Ecology and Environment Laboratory in Toulouse, France. Major ion concentrations were used in a mixing calculation as secondary check on fitted model parameters as described later in this section.

## 2.3. Stream Gauging and Catchment Delineation

We installed a stream gauging station at the outlet culvert. The gauging station consisted of two perforated PVC tubes fixed to the upstream and downstream headwalls of the culvert and armed with pressure transducers (Solinst Leveloggers®). Barometric compensation was performed using barometric pressure data from Solinst Barologgers® deployed nearby. Streamflow at the culvert was directly measured with a digital current meter at the time of installation and the observed flow was used to calibrate a value of Manning's  $n$ . The continuous record of water level slope and water depth, along with the culvert geometry and Manning's  $n$  coefficient were used to calculate flow according to Manning's equation (Dingman, 2002).

To determine the drainage area of the canal, we used lidar data obtained from the Brunei Survey Department and analyzed in GRASS GIS. We first filtered the lidar point cloud data to last-return points (using libLAS version 1.8.1, <http://liblas.org>). We then removed outliers among last-return points using two methods: (a) within each cell of a Cartesian grid, we removed outliers more than three times the interquartile range below the lower quartile (Tukey's fence) and recorded the value and location of the lowest among the remaining points; and (b) we removed points with large deviations from a bicubic spline surface through the points (using v.outlier, <https://grass.osgeo.org>). The remaining local minima were used to construct a gridded digital terrain model (DTM) for each of these sites by inverse-distance weighted interpolation using a geospatial translator library

(<https://gdal.org>). Once the smoothed DTM was created, we used the hydrological tools (flow accumulation and upslope area) in QGIS to delineate the catchment and calculate the area.

#### 2.4. Model Development

We developed a one-dimensional, isotope-enabled, reactive transport model for dissolved  $\text{CH}_4$  and  $\text{CO}_2$  as water flows along the canal that simulates several key processes (Figure 1b, Figure S1 in Supporting Information S1). Dissolved  $\text{CO}_2$  and  $\text{CH}_4$  gas are transported into the canal by groundwater advection (non-fractionating). Methane and  $\text{CO}_2$  are eliminated from the canal by degassing (non-fractionating). Microbial oxidation (Equation 1, fractionating, Hoyt, 2017) transforms methane to  $\text{CO}_2$ . Oxidation of dissolved organic carbon (DOC) oxidation (Equation 2, non-fractionating) also produces  $\text{CO}_2$ :



Methanogenesis in the canal water is considered negligible. Whatever  $\text{CH}_4$  and  $\text{CO}_2$  remain dissolved in the canal water at the outlet are lost as fluvial export.

Our approach extends a one-dimensional methane transport model by Heilweil et al. (2013, 2016) where  $\text{CH}_4$  concentrations along a canal provide information about the integrated methane fluxes upstream of the measurements. A similar approach is used by Pennington et al. (2018) to model  $\text{CO}_2$  and  $\text{O}_2$  concentrations along oxic streams and rivers to estimate  $\text{CO}_2$  emissions integrated along stream reaches. These models provide tools for using concentrations to estimate integrated fluxes along stream reaches that avoid problems caused by extreme variability in flux measurements from floating chambers. Heilweil et al. (2013, 2016) modified the work of Cook et al. (2003) to derive a mass balance expression of the change in dissolved methane load along a stream, which we also extend to  $\text{CO}_2$  (See Figure S1 in Supporting Information S1 for schematic):

$$\frac{dMQ}{dx} = qM_{\text{gw}} - \lambda_{\text{atm}}bw(M - M_{\text{eq}}) - \lambda_{\text{mic}}bwM \quad (3)$$

$$\frac{dCQ}{dx} = qC_{\text{gw}} - g\lambda_{\text{atm}}bw(C - C_{\text{eq}}) + \lambda_{\text{mic}}bwM + R \quad (4)$$

Where  $M$ ,  $M_{\text{gw}}$ , and  $M_{\text{eq}}$  are the concentration of methane in the canal water, the groundwater, and the concentration of methane that would be in equilibrium with the atmosphere, respectively ( $\text{mmol L}^{-1}$ ).  $C$ ,  $C_{\text{gw}}$ , and  $C_{\text{eq}}$  are the concentrations of  $\text{CO}_2$  in the canal, groundwater, and in equilibrium with the atmosphere, respectively ( $\text{mmol L}^{-1}$ ).  $Q$  is the streamflow ( $\text{m}^3 \text{s}^{-1}$ ), increasing with distance along the canal  $x$  (m),  $q$  is the rate of groundwater inflow per distance along the canal ( $\text{m}^3 \text{s}^{-1} \text{m}^{-1}$ ),  $b$  and  $w$  are the depth and width of the canal (m), respectively. Evaporation from the canal surface is assumed to be much smaller than stream outflow and is therefore neglected.  $R$  is the rate of conversion of DOC to  $\text{CO}_2$  through microbial and photo-oxidation ( $\text{m}^3 \text{s}^{-1} \text{m}^{-1} \text{mol m}^{-3}$  or  $\text{mol s}^{-1} \text{m}^{-1}$ ).  $\lambda_{\text{atm}}$  is the rate coefficient of methane degassing to the atmosphere for  $\text{CH}_4$  ( $\text{s}^{-1}$ ),  $g$  is a constant that relates atmospheric gas transfer coefficient for  $\text{CO}_2$  to the gas transfer coefficient for  $\text{CH}_4$ .  $g$  is equal to the ratio of Schmidt numbers for  $\text{CH}_4$  and  $\text{CO}_2$ , and is equal to 0.9667 (Wanninkhof, 1992). Including  $g$  in the model means that the degassing rate constant (and gas transfer velocity) for  $\text{CH}_4$  will be slightly higher than for  $\text{CO}_2$  at any given point to account for their different diffusion coefficients.  $\lambda_{\text{mic}}$  is the rate coefficient of methane oxidation to  $\text{CO}_2$ .

Assuming a uniform channel shape and uniform groundwater discharge along the channel:

$$Q(x) = qx \quad (5)$$

Which implies that  $dQ/dx = q$ . Since we wish to simulate gas concentrations along the canal ( $M$  and  $C$ ), we use the product rule to expand the left-hand side of Equations 3 and 4, substitute  $q$  for  $dQ/dx$  and isolate  $dM/dx$  and  $dC/dx$  (Heilweil et al., 2013). We also replace the product of the rate coefficients ( $\lambda_{\text{atm}}$  and  $\lambda_{\text{mic}}$ ) and the canal depth,  $b$ , with the gas transfer velocities  $V_{\text{atm}}$  and  $V_{\text{mic}}$  ( $\text{m s}^{-1}$ ) for degassing and microbial oxidation, respectively (Wanninkhof, 1992) to arrive at:

$$\frac{dM}{dx} = \frac{1}{qx} \{ q(M_{\text{gw}} - M) - V_{\text{atm}}w(M - M_{\text{eq}}) - V_{\text{mic}}wM \} \quad (6)$$

$$\frac{dC}{dx} = \frac{1}{qx} \{ q(C_{\text{gw}} - C) - gV_{\text{atm}}w(C - C_{\text{eq}}) + V_{\text{mic}}wM + R \} \quad (7)$$

#### 2.4.1. Composition of Incoming Porewater

In peat porewater, gas concentrations and  $\delta^{13}\text{C}$  vary with peat depth ( $z$ ). Therefore, the depth distribution of groundwater flow to the canal must be considered to produce representative values of  $M_{\text{gw}}$  and  $C_{\text{gw}}$ . We use an exponential function to characterize the depth distribution of groundwater flow to the canal given evidence that large voids and hollows near the peat surface drastically increase near-surface permeability in a near-exponential manner (Cobb et al., 2017). We considered alternative depth distributions for  $M_{\text{gw}}$  and  $C_{\text{gw}}$ , including the Kumaraswamy distribution (Kumaraswamy, 1980), that include a second, deep mode in groundwater input of methane and DIC, but found no evidence of this during statistical parameter estimation. A fitted parameter,  $D$ , defines how quickly flow diminishes with depth. The exponential distribution is truncated at the maximum depth of porewater sampling ( $z = 5.7$  m near the canal in this case) and normalized so that the area under the exponential curve is equal to 1 (normalization not shown in Equation 8 for clarity). The exponential equation is then multiplied by the porewater concentration at each depth, which is the result of linear interpolation of the observed porewater gas concentrations,  $M_{\text{obs}}$  and  $C_{\text{obs}}$ . The area under the resulting curve yields a representative concentration ( $M_{\text{gw}}$ ) of porewater entering the canal from all depths from the base of the peat to the water table:

$$M_{\text{gw}} = \int_0^z (e^{-Dz} \cdot (M_{\text{interp}}(z))) dz \quad (8)$$

where  $D$  (1/m) is a shape parameter that describes how lateral groundwater flow velocities decrease with depth and  $M_{\text{interp}}(z)$  interpolates the measured concentrations across depth.

#### 2.4.2. Gas Exchange Along the Canal

We parameterize degassing at the canal water surface with values of the gas exchange velocity estimated from fitting our model to  $\text{CO}_2$ ,  $\text{CH}_4$ , and  $\delta^{13}\text{C}$  concentrations along the canal (see Section 2.5), rather than attempting to measure small-scale characteristics of turbulence. In stream settings, gas exchange between the water and atmosphere depends primarily on flow velocity (Hall & Ulseth, 2020). As one moves downstream in the canal, the volumetric streamflow and flow velocity increase linearly, leading to an increase in the turbulent exchange of gases at the water surface. More turbulent exchange at the water surface leads to faster  $\text{CH}_4$  and  $\text{CO}_2$  degassing and faster diffusion of oxygen into the canal which facilitates faster methane and DOC oxidation. We apply the simplest interpretation of this fact and allow our fitted model parameters that are related to turbulent exchange at the water surface ( $V_{\text{atm}}$ ,  $V_{\text{mic}}$  and  $R$ ) to increase linearly with streamflow:

$$V_{\text{atm}}(x) = V_0 + sqx \quad (9)$$

$$V_{\text{mic}} = k_{\text{mic}} V_{\text{atm}} \quad (10)$$

$$R = k_{\text{DOC}} V_{\text{atm}} \quad (11)$$

where  $V_0$  is the atmospheric gas transfer velocity ( $\text{m s}^{-1}$ ) at the upstream end of the canal ( $x = 0$ ),  $s$  ( $\text{m}^{-2}$ ) is the coefficient that relates streamflow ( $Q = qx$ ) to the increase in  $V_{\text{atm}}$  along the canal,  $k_{\text{mic}}$  is a dimensionless coefficient that relates  $V_{\text{mic}}$  to  $V_{\text{atm}}$  and  $k_{\text{DOC}}$  ( $\text{mol m}^{-2}$ ) is a coefficient that relates  $R$  to  $V_{\text{atm}}$  and converts units. The canal is assumed to be under turbulent conditions which can be confirmed by calculating Reynolds number along the canal under the measured flow conditions.

#### 2.4.3. Isotope-Enabled Reactive Transport Model

We incorporate Equations 7 through 11 into the differential equations for methane and DIC concentration (Equations 5 and 6). We then re-write Equations 5 and 6 for each carbon isotopologue of interest:  $^{12}\text{CH}_4$ ,  $^{13}\text{CH}_4$ ,  $^{12}\text{CO}_2$ ,  $^{13}\text{CO}_2$  with respective concentrations denoted as  $M_{12}$ ,  $M_{13}$ ,  $C_{12}$ , and  $C_{13}$ , to arrive at our final model equations:

$$\frac{dM_{12}}{dx} = \frac{1}{qx} \{ q[M_{12\text{gw}} - M_{12}] - w[V_i + sqx][k_{\text{mic}}M_{12} + (M_{12} - M_{12\text{eq}})] \} \quad (12)$$



$$\frac{dM_{13}}{dx} = \frac{1}{qx} \left\{ q[M_{13\text{gw}} - M_{13}] - w[V_i + s q x] [\beta k_{\text{mic}} M_{13} + (M_{13} - M_{13\text{eq}})] \right\} \quad (13)$$

$$\frac{dC_{12}}{dx} = \frac{1}{qx} \left\{ q[C_{12\text{gw}} - C_{12}] + [V_i + s q x] [k_{\text{mic}} M_{12} w - \text{gw}(C_{12} - C_{12\text{eq}}) + k_{\text{DOC}}(1 - f)] \right\} \quad (14)$$

$$\frac{dC_{13}}{dx} = \frac{1}{qx} \left\{ q[C_{13\text{gw}} - C_{13}] + [V_i + s q x] [\beta k_{\text{mic}} M_{13} w - \text{gw}(C_{12} - C_{12\text{eq}}) + k_{\text{DOC}} f] \right\} \quad (15)$$

where  $\beta$  is a form of the isotopic fractionation factor for the microbial oxidation of methane (dimensionless) and is equal to the rate of oxidation of  $^{13}\text{CH}_4$  over the rate for  $^{12}\text{CH}_4$ .  $\beta$  is the inverse of the often-used fractionation factor,  $\alpha$ .  $f$  is the fraction of DOC that is  $^{13}\text{DOC}$  (dimensionless), estimated from measurements at a nearby field site (Gandois et al., 2013). Note that Equations 12 and 13 sum to Equation 6, and Equations 14 and 15 sum to Equation 7, because the total concentration is the sum of the concentrations of the two isotopologues. Our governing equations are written in terms of concentrations of the isotopologues which makes the isotopic mass balance easier to formulate. To compare our simulations to observed data we convert the isotope concentrations to  $\delta$  notation.

#### 2.4.4. Upper and Lower Bounds on Gas Concentrations, Isotopes and Fluxes

At both the upstream and far downstream limits of the canal, the values of concentration and isotope ratios are bounded by simple expressions which can be determined from our formulations. At the upstream boundary, where there is no flow, concentration gradients are zero and therefore differential Equations 5 and 6 for concentration simplify to algebraic equations. At  $x = 0$ ,  $V_{\text{atm}}$  is given by  $V_0$  and  $V_{\text{mic}}$  is given by  $k_{\text{mic}} V_0$  (Equations 9 and 10) and the differential Equations 6 and 7 simplify to:

$$M(x=0) = \frac{qM_{\text{gw}} + V_i w M_{\text{eq}}}{q + V_i w (1 + k_{\text{mic}})} \quad (16)$$

$$C(x=0) = \frac{qC_{\text{gw}} + V_i (qwC_{\text{eq}} + k_{\text{mic}} w M + k_{\text{doc}})}{q + gV_i w} \quad (17)$$

Simplifications for Equations 12–15 for isotopologues are included in Supporting Information S1.

If not for the effects of increasing water velocity on gas exchange (parameters  $V_{\text{atm}}$ ,  $V_{\text{mic}}$ , and  $R$ ), then the resulting concentrations and isotopic ratios of DIC and  $\text{CH}_4$  would remain uniform along the canal, equal to the values at the upstream boundary. From our field data, we know that concentration and isotopic ratios of DIC and  $\text{CH}_4$  change systematically (mostly monotonically) downstream along the canal, implying that one or more parameters must change along the canal.

As the flow increases downstream with the input of more groundwater, atmospheric gas exchange increases with turbulent mixing, and microbial oxidation grows to dominate over groundwater input so that the concentrations approach downstream bounding values. Taking the limit of  $M$  and  $C$  as  $x$  approaches infinity, gives:

$$\lim_{x \rightarrow \infty} M = \frac{M_{\text{eq}}}{(1 + k_{\text{mic}})} \quad (18)$$

$$\lim_{x \rightarrow \infty} C = C_{\text{eq}} + \frac{k_{\text{mic}} M_{\text{eq}}}{g(1 + k_{\text{mic}})} + \frac{k_{\text{doc}}}{\text{gw}} \quad (19)$$

These downstream bounding concentrations shows that, as flow accelerates in the channel, concentrations approach values that are independent of many of the parameters that control the upstream concentrations. The methane concentration approaches a value that is very low, less than  $M_{\text{eq}}$  (methane concentration in equilibrium with the atmosphere) and is independent of parameters except  $M_{\text{eq}}$  and  $k_{\text{mic}}$ , where the rate parameter  $k_{\text{mic}}$  is the only parameter that must be assessed from local data. DIC concentrations, on the other hand, approach a value that is larger than  $C_{\text{eq}}$  (DIC concentration in equilibrium with the atmosphere) and depends on  $C_{\text{eq}}$ ,  $k_{\text{mic}}$ ,  $M_{\text{eq}}$ ,  $k_{\text{doc}}$  and  $w$ .

Similarly, surface fluxes approach asymptotic values which can be calculated by plugging the above limits into the atmospheric flux terms of Equations 3 and 4 to get maximum downstream degassing fluxes ( $\phi_M$  and  $\phi_C$ ) per unit length of canal:

$$\phi_M = \text{wsq} \left[ \left( \lim_{x \rightarrow \infty} M \right) - M_{\text{eq}} \right] = -\text{wsq} \left( \frac{k_{\text{mic}}}{1 + k_{\text{mic}}} \right) \quad (20)$$

$$\phi_C = \text{gwsq} \left[ \left( \lim_{x \rightarrow \infty} C \right) - C_{\text{eq}} \right] = \text{wsq} M_{\text{eq}} \left( \frac{k_{\text{mic}}}{1 + k_{\text{mic}}} \right) + \text{sq} k_{\text{doc}} \quad (21)$$

Therefore, asymptotic concentrations and fluxes depend on only a subset of the model variables. However, all parameters are needed to determine how far downstream one needs to travel to approach the asymptotes.

## 2.5. Model Fitting

We estimated six parameters by fitting the four governing equations (Equations 12–15) to the observed canal data for concentration and  $\delta^{13}\text{C}$  of  $\text{CH}_4$  and  $\text{CO}_2$  using the Matlab multi-parameter non-linear regression function. By fitting all the different data types simultaneously, we achieve better estimates of parameters than we would if we fit only one data type. In particular, the isotope ratio measurements provide additional constraints beyond just concentrations while only introducing one additional parameter, the fractionation factor. The six parameters are: the shape parameter for lateral groundwater velocities,  $D$ , the isotopic fractionation factor,  $\beta$ , and coefficients used to calculate the rates of methane oxidation ( $k_{\text{mic}}$ ), degassing ( $s$  and  $V_0$ ), and DOC oxidation ( $k_{\text{DOC}}$ ). All the fitting parameters were assumed to be the same for the January and August datasets except  $D$  (how quickly groundwater flow diminishes with depth) and  $k_{\text{DOC}}$  (rate coefficient for DOC oxidation).  $D$  may vary because the contribution of deep groundwater may change with hydrologic conditions.  $k_{\text{DOC}}$  is allowed to vary because we expect that DOC entering the canal with porewater will change depending on hydrologic conditions, and oxidation rates to vary with flow conditions and solar radiation (photo-oxidation) in ways that are still poorly defined in the literature and our model is not equipped to calculate. From the best-fit parameters, we calculate the amounts of  $\text{CO}_2$  and  $\text{CH}_4$  that were advected into the canal, oxidized, degassed or remain dissolved in the canal water at the outflow.

## 2.6. Error Analysis and Uncertainty

Monte Carlo error propagation was used to estimate the uncertainty of the simulated  $\text{CO}_2$  and  $\text{CH}_4$  concentrations along the canal and overall canal gas budgets. The fitting algorithm provides the best-fit parameters and a confidence interval around each one. The better the model fit to observed data, the narrower the confidence intervals on the fitted parameters become. We used the best-fit parameter values and the covariance matrix produced by the fitting algorithm to generate 1,000 random parameter sets with a multi-Gaussian distribution, including covariances, around the fitted values. We use these parameter sets to run the model 1,000 times and then find the 95% confidence intervals ( $\text{CI}_{95}$ ) in the simulation results that captures the non-normally distributed (and non-symmetrical) confidence bands. These 95% confidence bands capture overall uncertainty associated with both model formulation and small-scale heterogeneities (like non-uniform groundwater input, small variations in canal dimension, etc.) that are not captured by the model.

## 2.7. Major Ion Mixing Calculations

As a secondary check on the contribution of deep porewater to the canal, we used major ion concentrations as conservative tracers. These solutes provide an independent estimate of the fitting parameter  $D$ . We applied the exponential flow distribution with depth (Equation 8) to the porewater ion data collected closest to the canal. Then, we optimize the value of  $D$  across all remaining ions simultaneously to produce the best match to observed canal ion concentrations.

# 3. Results and Discussion

## 3.1. $\text{CH}_4$ , DIC and $\delta^{13}\text{C}$ Indicate Upwelling of Deep Gas-Rich Porewater Beneath the Canal

In total, 93 porewater samples and 46 canal water samples were collected in Badas over two sampling campaigns in January and August 2020. In peat porewater, DIC and  $\text{CH}_4$  concentrations generally increase with depth

(Figure 3). All locations had gas concentrations below the ebullition threshold except for three that were close to the threshold. DIC is more enriched in  $^{13}\text{C}$  with depth.  $\text{CH}_4$  is depleted in both  $^{13}\text{C}$  and  $^2\text{H}$  in the first few meters below ground surface before becoming moderately enriched deeper in the peat profile (Figure 3 and Figure S3 in Supporting Information S1). The porewater profile through the canal showed the opposite trend where dissolved gas concentrations and  $\delta^{13}\text{C}$ -DIC were highest just below the canal bottom and decreased with depth. The few porewater samples collected in August 2020 at PT1-30W showed higher gas concentrations, slightly more enriched DIC and more depleted  $\text{CH}_4$  in the shallow groundwater compared to January 2020 samples at the same location (Figure S2 in Supporting Information S1).

The observed vertical patterns of increasing concentration and generally increasing  $\delta^{13}\text{C}$  of  $\text{CH}_4$  and DIC are consistent with methanogenesis and its carbon isotopic fractionation as porewater flows downward (Hoyt, 2017). We interpret the reversed trends in DIC and the carbon isotope ratios in DIC and  $\text{CH}_4$  in the peat below the canal bottom as a reversal in groundwater flow direction, where gas-rich groundwater is upwelling to discharge to the canal where hydraulic head is lowest.

### 3.2. $\text{CH}_4$ , DIC and $\delta^{13}\text{C}$ Show Consistent Trends Along Canal in Both Flow Conditions

Water samples along the canal were collected during two different flow conditions (Figure 4). In January 2020, the canal flow during sampling was lowest at  $0.24 \text{ m}^3/\text{s}$  and during the August 2020 sampling, canal flow was low-moderate at approximately  $0.31 \text{ m}^3/\text{s}$ . The hydrograph also characterizes the flashy nature of the canal flow where precipitation produces rapid spikes in flow. This is typical of the region's peatlands where the water table is consistently near the ground surface (Cobb & Harvey, 2019).

Canal methane, DIC and  $\delta^{13}\text{C}$  exhibit consistent, often monotonic trends along the canal. In both January and August 2020, dissolved gas concentrations in the canal decreased in the downstream direction (Figure 5) except for the sample at the flow divide in January 2020. Concentrations of  $\text{CH}_4$  become very small downstream of 3,750 (January) or 3,000 (August) meters. The furthest upstream (at the flow divide)  $\text{CH}_4$  and DIC concentrations in August were substantially higher than those observed in January.  $\delta^{13}\text{C}$  of DIC decreases (becomes isotopically depleted) in the downstream direction in both datasets except for the sample at the flow divide in January 2020.  $\delta^{13}\text{C}$  of  $\text{CH}_4$  initially increases to a maximum around 2,200 (January) or 1,200 (August) m downstream then decreases. The January canal data for  $\delta^{13}\text{C}$ - $\text{CH}_4$  shows a smoother trend than the August data. Where  $\text{CH}_4$  concentrations are very low, small methane inputs will have a strong impact on the overall  $\text{CH}_4$  isotopic signature which may explain the anomalously low  $\delta^{13}\text{C}$  of  $\text{CH}_4$  observed at 5,070 (January) and 4,880 (August).

DIC,  $\text{CH}_4$  and  $\delta^{13}\text{C}$  are all relatively uniform with depth in the canal water (Figure 5 and Figure S1a in Supporting Information S1). The shallow (30 cm below water surface) and deep (30 cm above canal bed) canal concentrations observed in August 2020 were similar, indicating that the canal is well mixed. In DIC,  $\text{CH}_4$ , and  $\delta^{13}\text{C}$ -DIC, substantial differences between the shallow and deep data occur only at 1,260 and 2,120 m.  $\delta^{13}\text{C}$ - $\text{CH}_4$  is generally more depleted in the deep samples which we attribute to groundwater inflow.

### 3.3. Fitted Model Indicates Spatial Patterns in Canal Methane Oxidation and Degassing

The model was fit simultaneously to observed concentrations and  $\delta^{13}\text{C}$  of  $\text{CH}_4$  and DIC (Figure 5) to estimate the parameters and their uncertainties (Table 1). We omitted 2 canal data points as outliers for the January data ( $x = 0$  and 5,070 m) and one point for the August data ( $x = 4,880$  m) because they showed markedly different values than the general trends. The root mean square error (RMSE) for modeled  $\text{CH}_4$  concentration in January (and August) was  $0.0100 \text{ mM}$  ( $0.00858 \text{ mM}$ ) and  $2.98\text{‰}$  ( $5.25\text{‰}$ ) for  $\delta^{13}\text{C}$ - $\text{CH}_4$ . The RMSE for the modeled  $\text{CO}_2$  concentration in January (and August) was  $0.0382 \text{ mM}$  ( $0.153 \text{ mM}$ ) and  $0.414\text{‰}$  ( $1.09\text{‰}$ ) for  $\delta^{13}\text{C}$ - $\text{CO}_2$ .

Fitted values of the parameter that describes the distribution of porewater velocity with depth,  $D_{\text{Jan}}$  and  $D_{\text{Aug}}$ , are almost identical, with standard deviations of uncertainty that overlap, indicating that the vertical distribution of porewater flow to the canal remains the same in low and moderate flow conditions with shallow ( $<1 \text{ m}$  deep) porewater contributing most of water discharge. However, since gas concentrations increase with depth within the peat, most of the methane advection to the canal comes from porewater between 0.5 and 2.5 m deep (Figure S4 in Supporting Information S1). The fitted fractionation factor for methane oxidation,  $\beta$ , of  $0.970 \pm 0.036$  was similar but slightly lower (more fractionating) than previously observed values by Teh et al. (2006) from 0.990

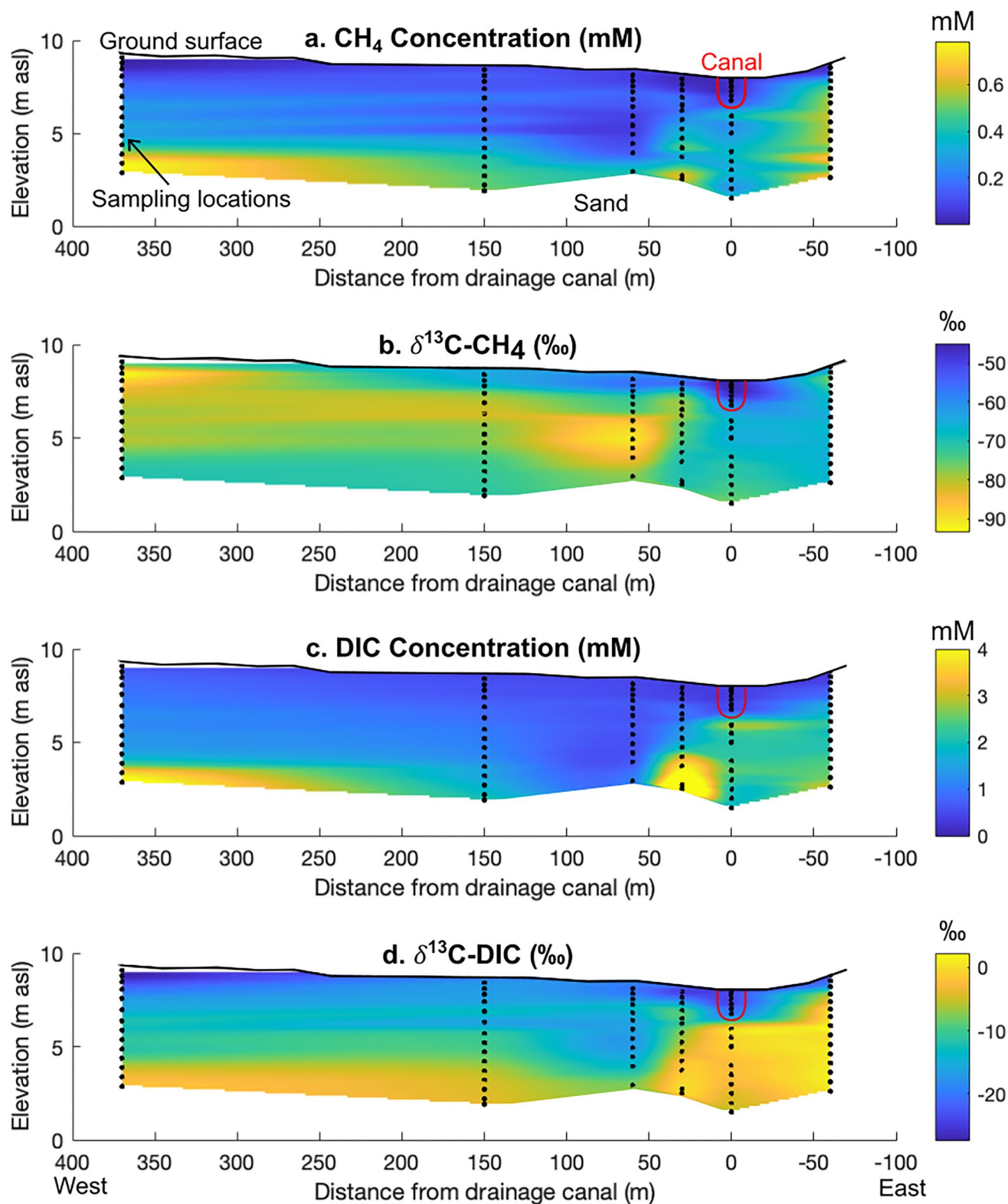


**Figure 3.** Peatland cross section along porewater sampling transect from January 2020 where black dots indicate sampling locations and the color indicates interpolated (a) CH<sub>4</sub> concentration, (b)  $\delta^{13}\text{C-CH}_4$ , (c) DIC concentration and (d)  $\delta^{13}\text{C-DIC}$ .

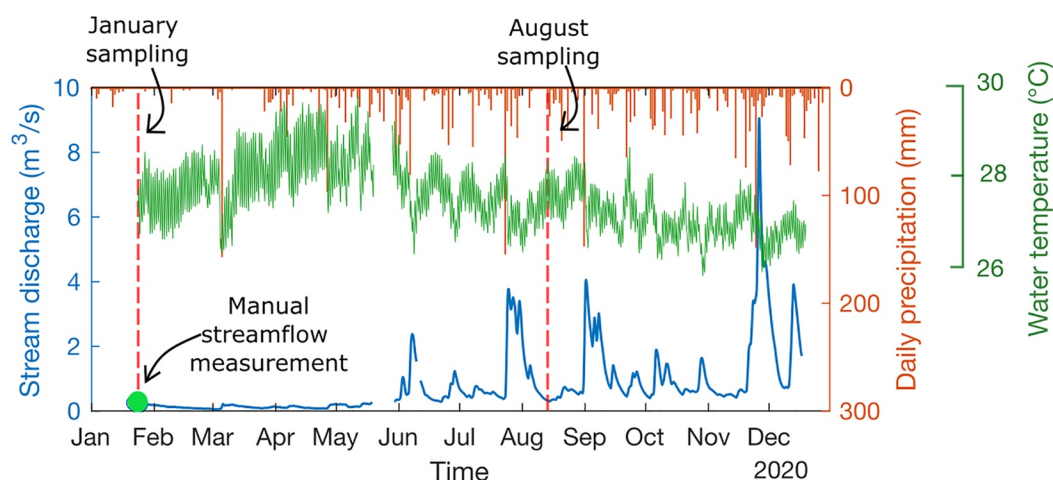


**Figure 4.** Hydrograph at the Badas Canal outlet, water temperature and daily precipitation for 2020 with sampling times indicated.

to 0.978 for tropical forest soils.  $K_{mic}$  is a coefficient that relates the rate of microbial oxidation of methane to the rate of degassing. The fitted value indicates that the microbial oxidation rate is higher than the rate of degassing.

The fitted model indicates that the rates of degassing, methane oxidation, and DOC oxidation all increase in the downstream direction in both January and August (Figure 6). At the far upstream end of the canal where water is stagnant, gas exchange velocities are very low. Moving downstream, the rate coefficients for degassing, methane oxidation and DOC oxidation ( $V_{atm}$ ,  $V_{mic}$ ,  $R$ ) all increase linearly which causes an asymptotic decrease in gas concentrations (Figure 5) and an increase in gas flux to the atmosphere (Figure 6). Therefore, it appears that gas exchange between the canal and the atmosphere is largely driven by flow-induced mixing and so becomes more important as the velocity increases downstream. While methane fluxes appear to have reached an asymptote (Figure 6) the model formulation shows that this is in fact a local maximum and that as  $x$  becomes very large, methane fluxes will theoretically decline toward the asymptote expressed in Equation 20, where the canal becomes a sink of methane from the atmosphere.

Ion concentrations in the canal and porewater (Figure S5 in Supporting Information S1) were low (e.g., mean chloride concentration of 3.7 mg/L) typical of ombrotrophic tropical peatlands in the region (Gandois et al., 2020). Higher concentrations of chloride, bromide, phosphate, sodium, potassium, magnesium and calcium were observed in deeper porewater with relatively high concentrations of magnesium, calcium and phosphate observed below the canal. We interpret this as upwelling of groundwater which has been in contact with mineral sediment and was, perhaps, channeled through the sand which underlies the peat.

The major ion concentrations and mixing calculation support the notion that there is porewater upwelling below the canal but that it makes a negligible contribution to canal flow. The low ion concentrations in the canal resembled those in the shallow porewater (Figure S5 in Supporting Information S1). For mixing analysis, we eliminated ions with observations below the detection limit (nitrite, sulfate, phosphate and ammonium). To estimate  $D$ , we optimized the exponential flow distribution with depth (Equation 8) for the remaining ions (fluoride, chloride, bromide, nitrate, phosphate, sodium, potassium, magnesium and calcium), which yielded a value of  $D = -1.42$ , similar to the value of  $-1.57$  fit using the carbon isotope model (Figure S4 in Supporting Information S1). This independent estimate of  $D$  confirms that most groundwater flow to the canal occurs in the shallow peat.

### 3.4. Methane Oxidation in Canal Dominates Over Emission

The fitted model provides a  $CH_4$  budget for the canal (Figure 7). In terms of canal inputs, substantially more  $CH_4$  was advected into the canal in August compared to January due to the higher rate of porewater discharge and to higher concentrations observed in the shallow porewater. Of the  $CH_4$  advected into the canal, the majority is oxidized (70%) and a smaller proportion is degassed to the atmosphere (26%). Very little  $CH_4$  input to the canal remains in the canal water at the outflow (4%).



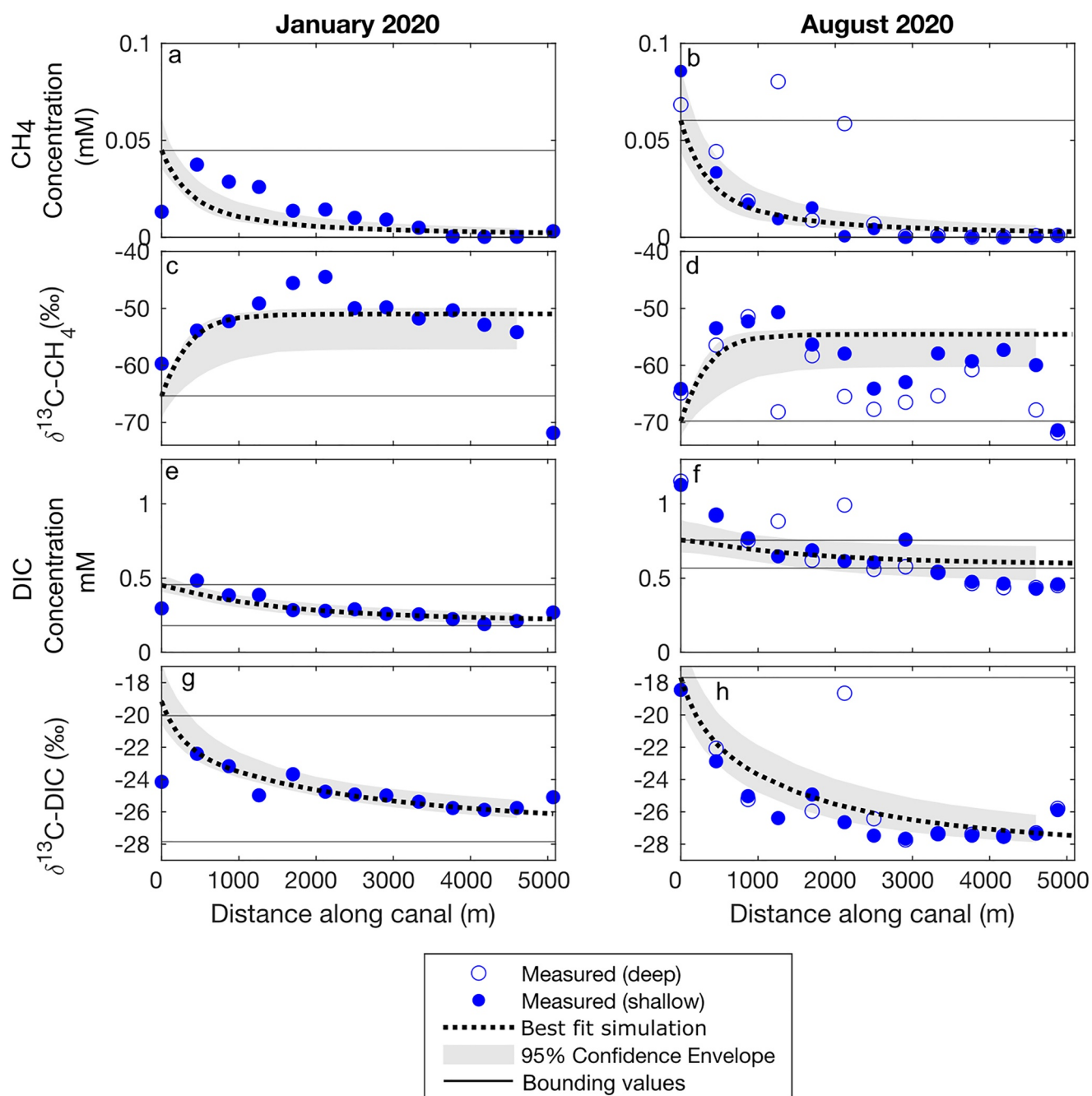


**Figure 5.** Measured and modeled concentrations of canal  $\text{CH}_4$  (a, b),  $\delta^{13}\text{C}-\text{CH}_4$  (c, d), concentration of DIC (e, f) and  $\delta^{13}\text{C}-\text{DIC}$  (g, h) in January (left column) and August (right column) 2020. Gray shading represents the 95% confidence intervals based on Monte Carlo simulations ( $n = 1,000$ ). Downstream bounding values for plots c, d and h are not shown because they are beyond the axis range.

The  $\text{CO}_2$  budget for the canal indicates that porewater advection (January: 42%, August: 26%) and DOC oxidation (January: 54%, August: 72%) were the dominant inputs of  $\text{CO}_2$  to the canal. By comparison, methane oxidation makes only a small contribution to canal  $\text{CO}_2$  inputs (January: 4%, August: 2%). Degassing is the largest output of  $\text{CO}_2$  (January: 80%, August: 79%), and the remaining dissolved  $\text{CO}_2$  exits the canal with streamflow and is transported toward the ocean (January: 20%, August: 21%).

Our simulated rate of methane degassing from the entire canal was  $4.19 \text{ mmol s}^{-1}$  ( $\text{CI}_{95}$ :  $2.56\text{--}9.48 \text{ mmol s}^{-1}$ ) or  $5,790 \text{ g CH}_4 \text{ d}^{-1}$  in January and  $6.60 \text{ mmol s}^{-1}$  ( $\text{CI}_{95}$ :  $3.83\text{--}15.8 \text{ mmol s}^{-1}$ ) or  $9,120 \text{ g CH}_4 \text{ d}^{-1}$  in August 2020.

**Table 1**  
*Model Parameters*

Fitted parameters			
Symbol	Parameter (unit)	Fitted value	Uncertainty (standard deviation)
$D_{Jan}$	Exponential coefficient to calculate depth distribution of incoming groundwater (dimensionless)	−1.56	0.144
$D_{Aug}$		−1.52	0.173
$\beta$	Isotopic fractionation factor of methane oxidation (dimensionless)	0.970	0.0036
$k_{mic}$	Rate coefficient for methane oxidation (dimensionless)	2.67	1.04
$V_0$	Initial rate of methane degassing ( $m\ d^{-1}$ )	0.0502	0.0162
$s$	Change in methane degassing rate along canal ( $m^{-2}$ )	$1.50\ e-7$	$3.32\ e-8$
$k_{DOC-Jan}$	Rate coefficient for oxidation of DOC ( $mol\ m^{-2}$ )	1.57	0.193
$k_{DOC-Aug}$		5.31	0.656
Input parameters			
Symbol	Parameter (unit)	Value	Source
$q$	Groundwater input rate per unit length of canal ( $m^2/s$ )	January: $4.890\ e-5$ August: $6.110\ e-5$	Field measurement of streamflow at canal outlet divided by canal length
$w$	Average width of canal (m)	10	Satellite imagery
$f$	Fraction of DOC that is $^{13}C$ DOC (dimensionless)	0.0107	Gandois et al., 2013
$M_{eq}$	Concentration of dissolved methane in equilibrium with the atmosphere (mM)	$2.68\ e-6$	Field measurement of atmospheric $CH_4$ concentration on site and converted to equilibrium concentration with Henry's Law.
$C_{eq}$	Concentration of dissolved Carbon Dioxide in equilibrium with the atmosphere (mM)	0.0176	Field measurement of atmospheric $CO_2$ concentration on site and converted to equilibrium concentration with Henry's Law.

Our model indicates that the amount of methane degassed from a drainage canal will increase with the amount of methane advected into the canal and therefore with canal drainage area. Therefore, we should also express the canal methane emission in terms of the canal drainage area: Per unit drainage area of the canal (divide the total emissions by the drainage area, 1,066 ha) the degassing rate is  $5.43\ g\ CH_4\ d^{-1}\ ha^{-1}$  in January and  $8.56\ g\ CH_4\ d^{-1}\ ha^{-1}$  in August. To facilitate comparison to studies that measure canal surface flux with floating chambers, we can also express the methane degassing rate as a flux from the water surface. However, this flux will depend on our estimated canal width, which has some random variability along the canal and in time. Therefore, we can use a range of widths from 4 to 30 m to provide a broad estimate of canal surface degassing flux (divide the

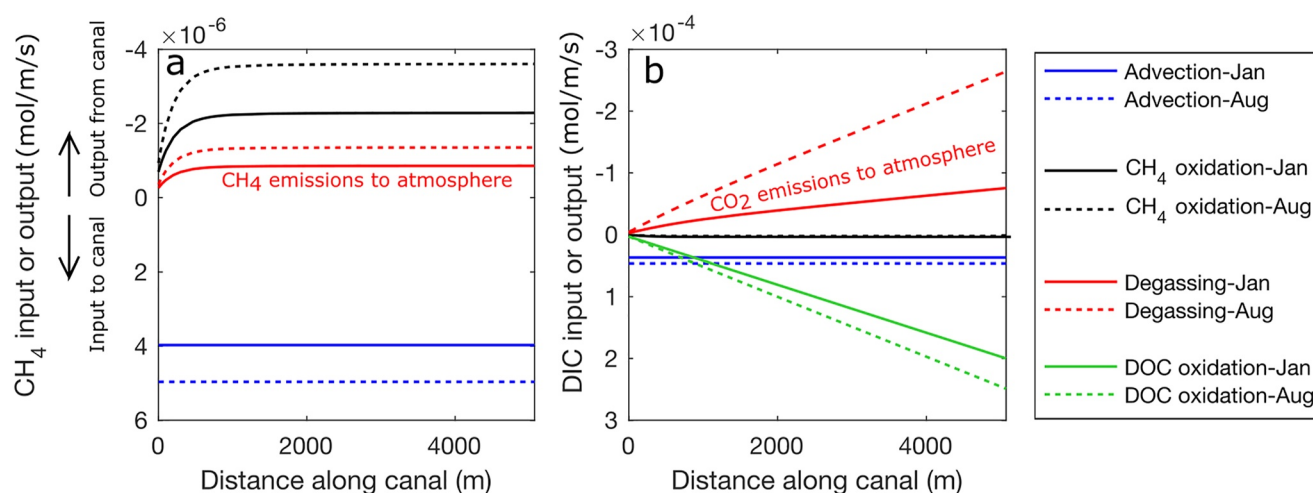


**Figure 6.** Simulated gas inputs and outputs along the length of the canal for (a)  $CH_4$  and (b) DIC.

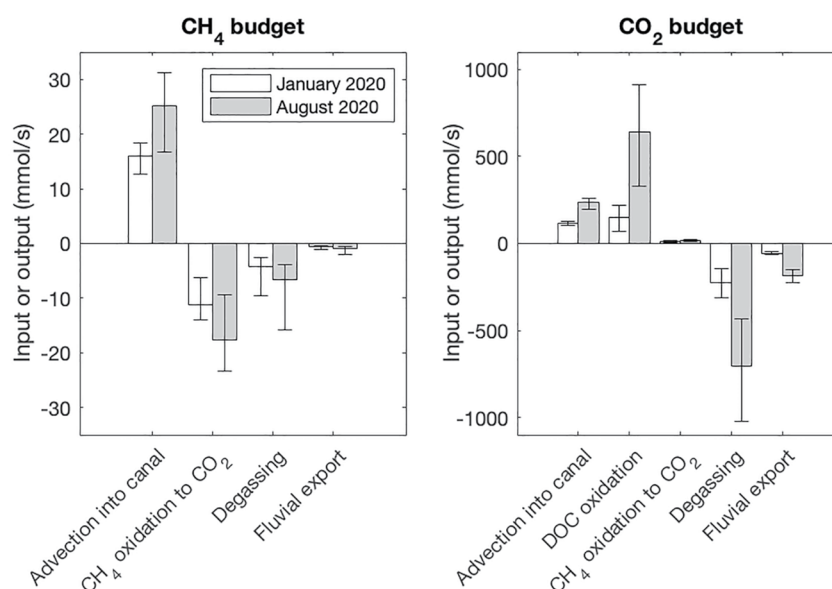


**Figure 7.** CH<sub>4</sub> (a) and CO<sub>2</sub> (b) budgets for the Badas Canal in January (white) and August (gray) 2020. Error bars represent the 95% confidence interval from Monte Carlo simulations ( $n = 1,000$ ).

total emissions by canal surface area) of 381–2,856 g CH<sub>4</sub> ha<sup>-1</sup> d<sup>-1</sup> in January and 600–4,500 g CH<sub>4</sub> ha<sup>-1</sup> d<sup>-1</sup> in August. The above numbers describe the average flux over the entire canal area. However, our fitted model indicates that degassing fluxes are very low near the flow divide where velocity is low (Figure 6).

Simulated CO<sub>2</sub> emissions from the entire canal were 852 kg/d in January and 2,680 kg/d in August 2020. This represents a higher rate of greenhouse gas emission than methane (in CO<sub>2</sub> equivalents) from the canal. However, the contribution of DOC oxidation to the canal CO<sub>2</sub> budget remains uncertain as indicated by the wide 95% confidence interval (Figure 6, Table S1 in Supporting Information S1). As a rough check on the DOC oxidation rate, we compare it to the rate of total organic carbon fluvial export from drainage canals in Malaysia (Cook et al., 2018) and find that our DOC oxidation rates fall on the same order of magnitude and below (9%–65%) TOC export from that study. We can also compare to a metadata analysis on peatland DOC export by Rosset et al. (2022) and find our DOC oxidation rate is on the same order of magnitude as the median tropical DOC export rate. Furthermore, our results indicate a substantial difference in the rate of DOC oxidation between January and August 2020. This could be caused by differing rates of photo-oxidation (photomineralization) of DOC depending on weather conditions (Gandois et al., 2019) and differing hydrologic conditions influencing the amount or quality of DOC transported to the canal (Cook et al., 2018; Martin et al., 2018). Previous research suggests photo-oxidation may be an important pathway for DOC mineralization in tropical peatland rivers given the observed recalcitrance of aquatic DOM in this region (Hodgkins et al., 2018; Nichols & Martin, 2021). Additionally, photosynthetic uptake of CO<sub>2</sub> by algae could impact the DIC concentration and  $\delta^{13}\text{C}$ -DIC (Finlay, 2004). However, the uncertainty in the DOC oxidation rate has minimal impact on the CH<sub>4</sub> budget.

### 3.5. Model Produces Comparable Canal Methane Fluxes to Other Studies

Our simulated rates of methane advection to the canal and canal degassing are in range of values estimated by Hoyt (2017) for a nearby pristine peatland in Brunei. Hoyt (2017) estimated that lateral groundwater transport of methane accounted for 53.7 g CH<sub>4</sub> ha<sup>-1</sup> d<sup>-1</sup> (per unit peatland area, not canal area). To compare, we divide our total advection rate to the Badas Canal by the catchment area to yield smaller but comparable values of 20.7 and 32.7 g CH<sub>4</sub> ha<sup>-1</sup> d<sup>-1</sup> for January and August, respectively. For degassing, Hoyt (2017) estimated that (per unit area of peatland) 15.6 g CH<sub>4</sub> ha<sup>-1</sup> d<sup>-1</sup> was degassed from the river. Again, we divide our total degassing rate by the catchment area to yield smaller values of 5.43 and 8.56 g CH<sub>4</sub> ha<sup>-1</sup> d<sup>-1</sup> for January and August, respectively. The difference in advection and degassing rates may be attributable to the fact that we calculate mostly shallow groundwater (methane poor) input to the canal, whereas Hoyt (2017) assumed peat porewater contribution to the river was uniform with depth.

**Table 2**  
*Methane Fluxes From Peatland Drainage Canal Surfaces in SE Asia*

Reference	Setting	Methane surface flux as reported	Methane flux converted to $\text{g CH}_4 \text{ ha}^{-1} \text{ d}^{-1}$
Jauhiainen and Silvennoinen (2012)	Cleared, drained then abandoned peatland in Central Kalimantan, Indonesia	$164 \text{ mg CH}_4 \text{ m}^{-2} \text{ d}^{-1}$	1,640
	Acacia wood plantation on peatlands in Sumatra, Indonesia:		
	Settled (undisturbed for ~5 years):	$1,073 \text{ mg CH}_4 \text{ m}^{-2} \text{ d}^{-1}$	10,730
	Recently disturbed:	$89 \text{ mg CH}_4 \text{ m}^{-2} \text{ d}^{-1}$	890
Kent (2019)	Channels through peat swamp forest in Central Kalimantan, Indonesia:		
	Intact peatlands:	$1.25\text{--}7.79 \text{ mg CH}_4\text{-C m}^{-2} \text{ d}^{-1}$	16.67–103.86
	Degraded peatlands:	$9.48\text{--}29.64 \text{ mg CH}_4\text{-C m}^{-2} \text{ d}^{-1}$	126.4–395.2
Manning et al. (2019)	Drainage ditch in oil palm plantations in Sarawak, Malaysia	$4.24 \text{ mg CH}_4\text{-C m}^{-2} \text{ hr}^{-1}$	1,356.8
Current study (Somers et al., 2022)	Partially drained and partially deforested peatland in Brunei		
	January:		381–2,856
	August:		600–4,500

Our calculated areal flux rate of methane emission from the Badas Canal surface (total emission/canal surface area) is also in range of the few canal methane flux observations that exist for SE Asia (Table 2) measured with floating chambers. While no similar studies to ours exist in the tropics, a recent study in a northern peatland estimated that 38%–87% of methane advected into a headwater stream was oxidized in the stream (Taillardat et al., 2022), bracketing our findings (70%). However, they did not find the same spatial patterns in  $\text{CH}_4$  and  $\text{CO}_2$ , possibly because the natural stream did not have a stagnant upstream area and had more variation in cross section.

### 3.6. Importance of Canal Methane Fluxes

Despite high rates of methanotrophy in the canal, our calculated canal areal methane flux is higher than most literature peat surface fluxes (Table S2 in Supporting Information S1) from SE Asian peatlands; Only 7 of 41 peat and vegetation fluxes exceed our minimum canal flux ( $381 \text{ g CH}_4 \text{ ha}^{-1} \text{ d}^{-1}$ ) and none exceeded our maximum flux ( $4,500 \text{ g CH}_4 \text{ ha}^{-1} \text{ d}^{-1}$ ). However, the canal covers only a small portion of the total catchment area, making the canal a substantial but not dominant source of methane in the Badas peatland.

In other peatlands, the type of peat landcover will determine the relative importance of canal methane emissions. We suggest canals are not the dominant source of methane emission in catchments dominated by intact peat swamp forest and burnt peatland (like Badas) given higher methane fluxes from these landcover types. However, canals are likely a more important contributor to total methane emissions in catchments dominated by drained forest and agriculture, as observed by Manning et al. (2019) on a palm plantation on peat soil in Sarawak, Malaysia. This is because tropical peatlands drained for agriculture exhibit lower methane fluxes than intact peat swamp forest. Our results suggest that drained peat surface methane fluxes must be accompanied by some measure of methane emitted through drainage canals to fully capture the carbon and climate implications of large-scale tropical peatland disruption. Inclusion of drainage canal emissions will improve the accuracy of GHG inventories for tropical peatlands overall.

The single-canal configuration of the Badas peatland lends itself to model development. However, typical drained tropical peatlands have denser canal networks, which may impact methane emissions. Canal mapping by Dadap et al. (2021) show the wide range of canal densities in the region, in places exceeding 5 km of drainage network per  $\text{km}^2$  of peatland. We expect the total amount of methane advected into drainage canals (per unit catchment area) to be similar under differing drainage densities. This is because we expect the mass of methane advected to canals to remain unchanged, given no change in methane production and peat surface fluxes. In other words, if a given catchment area had 10 canals, each canal would receive and emit one tenth the methane compared to one central canal that drained the same catchment area, yielding the same total emissions. However, differing drainage densities will impact the water table elevation and therefore anaerobic volume of the peat (Cobb et al., 2020), which would lead to a reduction in methane generation in densely drained peatlands.

Additionally, the relationship between canal cross section and discharge will create different levels of turbulence, potentially altering the balance between methane oxidation and emission in canals. Our study captures low-moderate flow conditions and future work should include investigation of canal methane dynamics under high flows and through varying canal cross-sections. We hypothesize that under high-flow conditions, more methane will be advected to the canal, resulting in higher methane emissions overall. Since turbulence drives both methane degassing and microbial oxidation (by increased oxygen concentration), more research is required to determine how much this ratio varies under different flow conditions and the method presented in this paper provides a valuable tool to do so.

### 3.7. Strengths and Limitations of the Approach

The isotope-enabled reactive transport modeling presented here provides a new method of estimating methane emissions from drainage canals that captures methane dynamics along the entire length of a canal. The model formulation and fit to empirical data provides new understanding of the processes that control canal methane emissions to the atmosphere and the spatial and temporal distribution of emissions. Our method complements the use of floating chambers, which require many measurements to be spatially and temporally representative. Furthermore, our use of carbon isotope modeling allows quantification of degassing versus oxidation beyond previous approaches (e.g., Heilweil et al., 2016) with important implications for peatland management and climate change. Our approach provides new insights into the mechanisms driving methane degassing and oxidation, namely turbulent gas exchange which increases with streamflow in the canal. The mathematical formulation also yields theoretical limits to canal gas concentrations and fluxes which can be easily applied to other field sites with only a subset of the data requirements.

Our model does not simulate ebullition since our observed concentrations of  $\text{CH}_4$  were almost all below the ebullition threshold. Floating chamber measurements can include methane emission from bubbling which may explain some of the high fluxes reported by Jauhiainen and Silvennoinen (2012). Our model does not capture gas transport by plants. Sedge mediated methane transport was observed to account for >70% of peat surface fluxes in a nearby disturbed peatland in Brunei (Akhtar et al., 2020). In sedge-filled canals, sedge-mediated transport of methane could potentially bypass the canal by channeling methane from the high-concentration porewater below the canal to the atmosphere through the plant's aerenchyma. Similarly, episodic methane bubbling may occur below the canal causing high methane fluxes that our model does not capture. However, the methane porewater concentrations observed in Badas were almost all below the threshold for ebullition (Figure S2 in Supporting Information S1).

### 3.8. Sources of Uncertainty

Our results showed longitudinal patterns in canal concentrations and isotopic ratios of DIC and  $\text{CH}_4$  that generally followed consistent trends that could be reproduced by our model. However, the model is, of course, a simplification of reality and that simplification leads to uncertainty in our results. Specifically, local scale heterogeneities along the canal can obscure the general trends and make it difficult to fit the model to field data without spatially-detailed model inputs. Local-scale heterogeneities include non-uniform groundwater inflow to the canal, changes in canal width, changes in peat thickness or the contribution of deeper groundwater, spatial differences in the concentrations and isotopic signature of  $\text{CO}_2$  and  $\text{CH}_4$  in porewater, exposure to wind (and therefore turbulent mixing) or sun and potentially differing microbial ecology (and therefore oxidation rates). For example, shading was recently linked to increased rates of methanotrophy in temperate rivers (Shelley et al., 2017). Our current approach is parsimonious and appropriate for the single, straight canal at our study site. However, drainage canals are often arranged in networks where some of these heterogeneities may become more important and should be investigated in future work.

By neglecting small-scale heterogeneities along the canal, our simulations achieve a worse fit to observed data. However, we think it is more compelling to use simple assumptions of uniformity and show that we can broadly explain the patterns and controlling factors and avoid the risk of overfitting the model. Our Monte Carlo error propagation captures the uncertainty in model results, including the heterogeneities mentioned above. The uncertainty is shown by the error bars and error envelopes in Figures 5 and 7, and Table 1, that represent the 95% confidence intervals. Our model is fit to eight datasets (corresponding to the panels in Figure 5) instead of one. This is why more than 5% of the observed datapoints can fall outside the 95% confidence envelope.



In our data, local heterogeneities seemed to be most obvious in the  $\delta^{13}\text{C}\text{-CH}_4$  data that was collected in August 2020, which does not follow a monotonic trend. When  $\delta^{13}\text{C}\text{-CH}_4$  cannot be well matched by the model, parameter uncertainties become larger and our ability to differentiate between methane oxidation and degassing is reduced.  $\delta^{13}\text{C}\text{-CO}_2$  observations should provide an additional constraint on methane oxidation rates because lighter methane is preferentially oxidized to create lighter  $\text{CO}_2$ . However, we found that DOC oxidation also introduced isotopically depleted  $\text{CO}_2$  and obscured the impact of methane oxidation. Additional sampling of DOC concentrations and isotopic ratios would help to constrain DOC oxidation and differentiate between the isotopic influence of  $\text{CH}_4$  and DOC oxidation on  $\delta^{13}\text{C}\text{-CO}_2$ .

#### 4. Conclusions

We developed an isotope-enabled  $\text{CO}_2$  and  $\text{CH}_4$  mass-balance model for tropical peatland drainage canals and applied it to two datasets from the Badas Canal in Brunei Darussalam. Our results inform our conceptual model of methane dynamics in tropical peatland drainage canals (Figure 1). Shallow porewater dominates groundwater inflow to the canal given the higher hydraulic conductivity of the shallow peat. Deeper porewater also flows toward the canal and upwells near the canal but contributes little to canal flow. In the canal, the majority of the incoming methane is oxidized to  $\text{CO}_2$  by microbes (70%). A smaller, but still substantial amount of methane is degassed to the atmosphere at the canal surface (26%) and a small amount remains dissolved in the canal where it exits the peatland (4%). Our estimated areal methane flux from the drainage canal surface is larger than most observed tropical peat surface fluxes. However, drainage canals cover a relatively small area, making them a substantial but not dominant methane source in the peatland.

Our empirical field data and fitted mathematical model provide new understanding of the processes controlling methane emissions from canals. More methane is emitted from drainage canals during periods of moderate flow compared to low flow, even if the oxidized fraction remains constant, as more methane is transported to the canal. At the upstream end of the canal, streamflow and therefore turbulence is very low, producing little gas exchange ( $\text{CH}_4$  and oxygen) at the canal surface. This limits both methane degassing and methane oxidation at the upstream end of the canal leaving higher dissolved  $\text{CH}_4$  concentrations. Downstream, the rate of gas exchange increases, and dissolved gas concentrations decrease asymptotically until—eventually—dissolved methane concentration will no longer depend on porewater concentration or input. Our results reveal the fate of laterally transported methane in a disturbed tropical peatland and clarify the net impact of widespread peatland drainage on methane emissions.

#### Conflict of Interest

The authors declare no conflicts of interest relevant to this study.

#### Data Availability Statement

Field data and Matlab model codes (Somers et al., 2023) for this study are available without registration from the HydroShare repository at <https://doi.org/10.4211/hs.3953b24e0238467980a226c72cfc360e>. Matlab model files (Somers et al., 2022) are also available without registration from GitHub at [https://github.com/Lauren-Somers/Badas\\_Methane](https://github.com/Lauren-Somers/Badas_Methane).

#### References

- Adji, F., Hamada, Y., Darung, U., Limin, S., & Hatano, R. (2014). Effect of plant-mediated oxygen supply and drainage on greenhouse gas emission from a tropical peatland in Central Kalimantan, Indonesia. *Soil Science & Plant Nutrition*, 60(2), 216–230. <https://doi.org/10.1080/00380768.2013.872019>
- Akhtar, H., Lupascu, M., Sukri, R. S., Smith, T. E. L., Cobb, A. R., & Swarup, S. (2020). Significant sedge-mediated methane emissions from degraded tropical peatlands. *Environmental Research Letters*, 16. <https://doi.org/10.1088/1748-9326/abc7dc>
- Bange, H. W., Sim, C. H., Bastian, D., Kallert, J., Kock, A., Mujahid, A., & Müller, M. (2019). Nitrous oxide ( $\text{N}_2\text{O}$ ) and methane ( $\text{CH}_4$ ) in rivers and estuaries of northwestern Borneo. *Biogeosciences*, 16(22), 4321–4335. <https://doi.org/10.5194/bg-16-4321-2019>
- Cobb, A. R., Dommain, R., Tan, F., Heng, N. H. E., & Harvey, C. F. (2020). Carbon storage capacity of tropical peatlands in natural and artificial drainage networks. *Environmental Research Letters*, 15(11), 114009. <https://doi.org/10.1088/1748-9326/aba867>
- Cobb, A. R., & Harvey, C. F. (2019). Scalar simulation and parameterization of water table dynamics in tropical peatlands. *Water Resources Research*, 55(11), 9351–9377. <https://doi.org/10.1029/2019WR025411>

#### Acknowledgments

The authors thank Jeffery Muli anak Incham, Ramasamy anak Zulkiflee, Haji Bohari bin Haji Idi and Surin Kumar Thamilselvan for field assistance; Jonathan Davies, Shuhei Ono and Richard Doucett for helpful discussions and technical guidance; the Brunei Forestry Department for permission to conduct research at Badas (JPH/UND/17) and export permits; Brunei Shell Petroleum Co Sdn Bhd for site access and discussions; Frédéric Julien at the PAPC platform for major elements analysis (EcoLab Laboratory). This research was supported by the National Research Foundation Singapore under Grant NRF2016-IT-COO1-021, the US National Science Foundation under Grant 1923491, and the Natural Science and Engineering Research Council of Canada.

- Cobb, A. R., Hoyt, A. M., Gandois, L., Eri, J., Dommain, R., Salim, K. A., et al. (2017). How temporal patterns in rainfall determine the geomorphology and carbon fluxes of tropical peatlands. *Proceedings of the National Academy of Sciences of the United States of America*, 114(26), E5187–E5196. <https://doi.org/10.1073/pnas.1701090114>
- Cook, P. G., Favreau, G., Dighton, J. C., & Tickell, S. (2003). Determining natural groundwater influx to a tropical river using radon, chlorofluorocarbons and ionic environmental tracers. *Journal of Hydrology*, 277(1–2), 74–88. [https://doi.org/10.1016/s0022-1694\(03\)00087-8](https://doi.org/10.1016/s0022-1694(03)00087-8)
- Cook, S., Whelan, M. J., Evans, C. D., Gauci, V., Peacock, M., Garnett, M. H., et al. (2018). Fluvial organic carbon fluxes from oil palm plantations on tropical peatland. *Biogeosciences*, 15(24), 7435–7450. <https://doi.org/10.5194/bg-15-7435-2018>
- Couwenberg, J., Dommain, R., & Joosten, H. (2010). Greenhouse gas fluxes from tropical peatlands in south-east Asia. *Global Change Biology*, 16(6), 1715–1732. <https://doi.org/10.1111/j.1365-2486.2009.02016.x>
- Crawford, J. T., Lottig, N. R., Stanley, E. H., Walker, J. F., Hanson, P. C., Finlay, J. C., & Striegl, R. G. (2014). CO<sub>2</sub> and CH<sub>4</sub> emissions from streams in a lake-rich landscape: Patterns, controls, and regional significance. *Global Biogeochemical Cycles*, 28(3), 197–210. <https://doi.org/10.1002/2013GB004661>
- Dadap, N. C., Hoyt, A. M., Cobb, A. R., Oner, D., Kozinski, M., Fua, P. V., et al. (2021). Drainage canals in Southeast Asian peatlands increase carbon emissions. *AGU Advances*, 2(1), e2020AV000321. <https://doi.org/10.1029/2020AV000321>
- Dadap, N. C., Cobb, A. R., Hoyt, A. M., Harvey, C. F., & Konings, A. G. (2019). Satellite soil moisture observations predict burned area in Southeast Asian peatlands. *Environmental Research Letters*, 14(9), 094014. <https://doi.org/10.1088/1748-9326/ab3891>
- Deshmukh, C. S., Julius, D., Evans, C. D., NardiSusanto, A. P., Page, S. E., Gauci, V., et al. (2020). Impact of forest plantation on methane emissions from tropical peatland. *Global Change Biology*, 26(4), 2477–2495. <https://doi.org/10.1111/gcb.15019>
- Dhandapani, S., Ritz, K., Evers, S., Yule, C. M., & Sjögersten, S. (2019). Are secondary forests second-rate? Comparing peatland greenhouse gas emissions, chemical and microbial community properties between primary and secondary forests in Peninsular Malaysia. *Science of the Total Environment*, 655, 220–231. <https://doi.org/10.1016/j.scitotenv.2018.11.046>
- Dingman, S. L. (2002). *Physical hydrology* (2nd ed.). Waveland Press Incorporated.
- Dommain, R., Cobb, A. R., Joosten, H., Glaser, P. H., Chua, A. F. L., Gandois, L., et al. (2015). Forest dynamics and tip-up pools drive pulses of high carbon accumulation rates in a tropical peat dome in Borneo (Southeast Asia). *Journal of Geophysical Research: Biogeosciences*, 120(4), 617–640. <https://doi.org/10.1002/2014JG002796>
- Field, R. D., Van Der Werf, G. R., & Shen, S. S. P. P. (2009). Human amplification of drought-induced biomass burning in Indonesia since 1960. *Nature Geoscience*, 2(3), 185–188. <https://doi.org/10.1038/ngeo443>
- Finlay, J. C. (2004). Patterns and controls of lotic algal stable carbon isotope ratios. *Limnology & Oceanography*, 49(3), 850–861. <https://doi.org/10.4319/lo.2004.49.3.0850>
- Furukawa, Y., Inubushi, K., Ali, M., Itang, A. M., & Tsuruta, H. (2005). Effect of changing groundwater levels caused by land-use changes on greenhouse gas fluxes from tropical peat lands. *Nutrient Cycling in Agroecosystems*, 71(1), 81–91. <https://doi.org/10.1007/s10705-004-5286-5>
- Gandois, L., Cobb, A. R., Hei, I. C., Lim, L. B. L., Salim, K. A., & Harvey, C. F. (2013). Impact of deforestation on solid and dissolved organic matter characteristics of tropical peat forests: Implications for carbon release. *Biogeochemistry*, 114(1–3), 183–199. <https://doi.org/10.1007/s10533-012-9799-8>
- Gandois, L., Hoyt, A. M., Mounier, S., Le Roux, G., Harvey, C. F., Claustres, A., et al. (2019). From canals to the coast: Dissolved organic matter and trace metal composition in rivers draining degraded tropical peatlands in Indonesia. *Biogeosciences Discussions*, 17(7), 1897–1909. <https://doi.org/10.5194/bg-2019-253>
- Gandois, L., Hoyt, A. M., Mounier, S., Roux, G. L., Harvey, C. F., Claustres, A., et al. (2020). From canals to the coast: Dissolved organic matter and trace metal composition in rivers draining degraded tropical peatlands in Indonesia. *Biogeosciences*, 17(7), 1897–1909. <https://doi.org/10.5194/bg-17-1897-2020>
- Hadi, A., Inubushi, K., Furukawa, Y., Purnomo, E., Rasmadi, M., & Tsuruta, H. (2005). Greenhouse gas emissions from tropical peatlands of Kalimantan, Indonesia. *Nutrient Cycling in Agroecosystems*, 71(1), 73–80. <https://doi.org/10.1007/s10705-004-0380-2>
- Hall, R. O., & Ulseth, A. J. (2020). Gas exchange in streams and rivers. *WIREs Water*, 7(1), 1–18. <https://doi.org/10.1002/wat2.1391>
- Heilweil, V. M., Solomon, D. K., Darrah, T. H., Gilmore, T. E., & Genereux, D. P. (2016). Gas-tracer experiment for evaluating the fate of methane in a coastal plain stream: Degassing versus in-stream oxidation. *Environmental Science and Technology*, 50(19), 10504–10511. <https://doi.org/10.1021/acs.est.6b02224>
- Heilweil, V. M., Stolp, B. J., Kimball, B. A., Susong, D. D., Marston, T. M., & Gardner, P. M. (2013). A stream-based methane monitoring approach for evaluating groundwater impacts associated with unconventional gas development. *Groundwater*, 51(4), 511–524. <https://doi.org/10.1111/gwat.12079>
- Hirano, T., Jauhainen, J., Inoue, T., & Takahashi, H. (2009). Controls on the carbon balance of tropical peatlands. *Ecosystems*, 12(6), 873–887. <https://doi.org/10.1007/s10021-008-9209-1>
- Hirano, T., Segah, H., Harada, T., Limin, S., June, T., Hirata, R., & Osaki, M. (2007). Carbon dioxide balance of a tropical peat swamp forest in Kalimantan, Indonesia. *Global Change Biology*, 13(2), 412–425. <https://doi.org/10.1111/j.1365-2486.2006.01301.x>
- Hodgkins, S. B., Richardson, C. J., Dommain, R., Wang, H., Glaser, P. H., Verbeke, B., et al. (2018). Tropical peatland carbon storage linked to global latitudinal trends in peat recalcitrance. *Nature Communications*, 9(1), 3640. <https://doi.org/10.1038/s41467-018-06050-2>
- Holmes, M. E., Chanton, J. P., Tfaily, M. M., & Ogram, A. (2015). CO<sub>2</sub> and CH<sub>4</sub> isotope compositions and production pathways in a tropical peatland. *Global Biogeochemical Cycles*, 29, 1–18. <https://doi.org/10.1002/2014GB004951>
- Hooijer, A., Page, S., Canadell, J. G., Silvius, M., Kwadijk, J., Wosten, J., & Jauhainen, J. (2010). Current and future CO<sub>2</sub> emissions from drained peatlands in Southeast Asia. *Biogeosciences*, 7(5), 1505–1514. <https://doi.org/10.5194/bg-7-1505-2010>
- Hooijer, A., Page, S., Jauhainen, J., Lee, W. A., Lu, X. X., Idris, A., & Anshari, G. (2012). Subsidence and carbon loss in drained tropical peatlands. *Biogeosciences*, 9(3), 1053–1071. <https://doi.org/10.5194/bg-9-1053-2012>
- Hoyt, A. M. (2017). *Carbon fluxes from tropical peatlands: Methane, carbon dioxide, and peatland subsidence*. (Doctoral dissertation). Massachusetts Institute of Technology.
- Hoyt, A. M., Chaussard, E., Seppäläinen, S. S., & Harvey, C. F. (2020). Widespread subsidence and carbon emissions across Southeast Asian peatlands. *Nature Geoscience*, 13(6), 435–440. <https://doi.org/10.1038/s41561-020-0575-4>
- Hoyt, A. M., Gandois, L., Eri, J., Kai, F. M., Harvey, C. F., & Cobb, A. R. (2019). CO<sub>2</sub> emissions from an undrained tropical peatland: Interacting influences of temperature, shading and water table depth. *Global Change Biology*, 25(9), 2885–2899. <https://doi.org/10.1111/gcb.14702>
- Inubushi, K., Furukawa, Y., Hadi, A., Purnomo, E., & Tsuruta, H. (2003). Seasonal changes of CO<sub>2</sub>, CH<sub>4</sub> and N<sub>2</sub>O fluxes in relation to land-use change in tropical peatlands located in coastal area of South Kalimantan. *Chemosphere*, 52(3), 603–608. [https://doi.org/10.1016/S0045-6535\(03\)00242-X](https://doi.org/10.1016/S0045-6535(03)00242-X)
- Ishikura, K., Darung, U., Inoue, T., & Hatano, R. (2018). Variation in soil properties regulate greenhouse gas fluxes and global warming potential in three land use types on tropical peat. *Atmosphere*, 9(12), 465. <https://doi.org/10.3390/atmos9120465>

- Ishikura, K., Hirata, R., Hirano, T., Okimoto, Y., Wong, G. X., Melling, L., et al. (2019). Carbon dioxide and methane emissions from peat soil in an undrained tropical peat swamp forest. *Ecosystems*, 22(8), 1852–1868. <https://doi.org/10.1007/s10021-019-00376-8>
- Jauhiainen, J., Limin, S., Silvennoinen, H., & Yasander, H. (2008). Carbon dioxide and methane fluxes in drained tropical peat before and after hydrological restoration. *Ecology*, 89(12), 3503–3514. <https://doi.org/10.1890/07-2038.1>
- Jauhiainen, J., & Silvennoinen, H. (2012). Diffusion GHG fluxes at tropical peatland drainage canal water surfaces. *Suo*, 63(3–4), 93–105.
- Jauhiainen, J., Takahashi, H., Heikkinen, J. E. P., Martikainen, P. J., & Vasander, H. (2005). Carbon fluxes from a tropical peat swamp forest floor. *Global Change Biology*, 11(10), 1788–1797. <https://doi.org/10.1111/j.1365-2486.2005.001031.x>
- Kent, M. (2019). *Greenhouse gas emissions from channels draining intact and degraded tropical peat swamp forest*. [Doctoral dissertation]. The Open University. <https://doi.org/10.21954/ou.ro.00000704>
- Kumaraswamy, P. (1980). A generalized probability density function for double-bounded random processes. *Journal of Hydrology*, 46(1–2), 79–88. [https://doi.org/10.1016/0022-1694\(80\)90036-0](https://doi.org/10.1016/0022-1694(80)90036-0)
- Limpens, J., Berendse, F., Blodau, C., Canadell, J. G., Freeman, C., Holden, J., et al. (2008). Peatlands and the carbon cycle: From local processes to global implications - a synthesis. *Biogeosciences*, 5(5), 1475–1491. <https://doi.org/10.5194/bg-5-1475-2008>
- Lupascu, M., Akhtar, H., Smith, T. E. L., & Sukri, R. S. (2020). Post-fire carbon dynamics in the tropical peat swamp forests of Brunei reveal long-term elevated CH<sub>4</sub> flux. *Global Change Biology*, 26(9), 5125–5145. <https://doi.org/10.1111/gcb.15195>
- Manning, F. C., Kho, L. K., Hill, T. C., Cornulier, T., & Teh, Y. A. (2019). Carbon emissions from oil palm plantations on peat soil. *Frontiers in Forests and Global Change*, 2. <https://doi.org/10.3389/ffgc.2019.00037>
- Martin, P., Cherukuru, N., Tan, A. S. Y., Sanwani, N., Mujahid, A., & Müller, M. (2018). Distribution and cycling of terrigenous dissolved organic carbon in peatland-draining rivers and coastal waters of Sarawak, Borneo. *Biogeosciences*, 15(22), 6847–6865. <https://doi.org/10.5194/bg-15-6847-2018>
- Melling, L., Hatano, R., & Kah, J. G. (2005). Methane fluxes from three ecosystems in tropical peatland of Sarawak, Malaysia. *Soil Biology and Biochemistry*, 37(8), 1445–1453. <https://doi.org/10.1016/j.soilbio.2005.01.001>
- Miettinen, J., Hooijer, A., Vernimmen, R., Liew, S. C., & Page, S. E. (2017). From carbon sink to carbon source: Extensive peat oxidation in insular southeast Asia since 1990. *Environmental Research Letters*, 12(2), 024014. <https://doi.org/10.1088/1748-9326/aa5b6f>
- Miettinen, J., Shi, C., & Liew, S. C. (2016). Land cover distribution in the peatlands of Peninsular Malaysia, Sumatra and Borneo in 2015 with changes since 1990. *Global Ecology and Conservation*, 6, 67–78. <https://doi.org/10.1016/j.gecco.2016.02.004>
- Nichols, R. S., & Martin, P. (2021). Low biodegradability of dissolved organic matter from southeast Asian peat-draining rivers. *Journal of Geophysical Research: Biogeosciences*, 126(6). <https://doi.org/10.1029/2020JG006182>
- Page, S., Hoscilo, A., Langner, A., Tansey, K., Siegert, F., Limin, S., & Rieley, J. (2009). Tropical peatland fires in Southeast Asia. In *Tropical fire ecology* (pp. 263–287). Springer Praxis Books. [https://doi.org/10.1007/978-3-540-77381-8\\_9](https://doi.org/10.1007/978-3-540-77381-8_9)
- Page, S., Rieley, J. O., & Banks, C. J. (2011). Global and regional importance of the tropical peatland carbon pool. *Global Change Biology*, 17(2), 798–818. <https://doi.org/10.1111/j.1365-2486.2010.02279.x>
- Pangala, S. R., Moore, S., Hornibrook, E. R. C., & Gauci, V. (2013). Trees are major conduits for methane egress from tropical forested wetlands. *New Phytologist*, 197(2), 524–531. <https://doi.org/10.1111/nph.12031>
- Pennington, R., Argerich, A., & Haggerty, R. (2018). Measurement of gas exchange rate in streams by the oxygen-carbon method. *Freshwater Science*, 37(2), 222–237. <https://doi.org/10.1086/698018>
- Rosset, T., Binet, S., Rigal, F., & Gandois, L. (2022). Peatland dissolved organic carbon export to surface waters: Global significance and effects of anthropogenic disturbance. *Geophysical Research Letters*, 49(5), e2021GL096616. <https://doi.org/10.1029/2021GL096616>
- Sakabe, A., Itoh, M., Hirano, T., & Kusin, K. (2018). Ecosystem-scale methane flux in tropical peat swamp forest in Indonesia. *Global Change Biology*, 24(11), 5123–5136. <https://doi.org/10.1111/gcb.14410>
- Sanci, R., & Panarello, H. O. (2015). Carbon and hydrogen isotopes as tracers of methane dynamic in wetlands. *International Journal of Geosciences*, 6(07), 720–728. <https://doi.org/10.4236/ijg.2015.67058>
- Shelley, F., Ings, N., Hildrew, A. G., Trimmer, M., & Grey, J. (2017). Bringing methanotrophy in rivers out of the shadows. *Limnology & Oceanography*, 62(6), 2345–2359. <https://doi.org/10.1002/lno.10569>
- Sjögersten, S., Siegenthaler, A., Lopez, O. R., Aplin, P., Turner, B., & Gauci, V. (2020). Methane emissions from tree stems in neotropical peatlands. *New Phytologist*, 225(2), 769–781. <https://doi.org/10.1111/nph.16178>
- Somers, L., Hoyt, A., Cobb, A. R., Isnin, S., Suhup, M. A., Sukri, R. S., et al. (2022). Badas\_Methane [software]. GitHub. [https://github.com/Lauren-Somers/Badas\\_Methane](https://github.com/Lauren-Somers/Badas_Methane)
- Somers, L., Hoyt, A., Cobb, A. R., Isnin, S., Suhup, M. A., Sukri, R. S., et al. (2023). Peatland canal methane data from Badas, Brunei Darussalam [dataset]. HydroShare. <https://doi.org/10.4211/h.s.3953b24e0238467980a226c72cfc360e>
- Suhup, M. A. B. H., Gödeke, S. H., Cobb, A. R., & Sukri, R. S. (2020). Seismic refraction study, single well test and physical core analysis of anthropogenic degraded Peat at the Badas Peat Dome, Brunei Darussalam. *Engineering Geology*, 273, 105689. <https://doi.org/10.1016/j.enggeo.2020.105689>
- Taillardat, P., Bodmer, P., Deblois, C. P., Ponçot, A., Prijac, A., Riahi, K., et al. (2022). Carbon dioxide and methane dynamics in a peatland headwater stream: Origins, processes and implications. *Journal of Geophysical Research: Biogeosciences*, 127(7). <https://doi.org/10.1029/2022JG006855>
- Tang, A. C. I., Stoy, P. C., Hirata, R., Musin, K. K., Aeries, E. B., Wenceslaus, J., & Melling, L. (2018). Eddy covariance measurements of methane flux at a tropical peat forest in Sarawak, Malaysian Borneo. *Geophysical Research Letters*, 45(9), 4390–4399. <https://doi.org/10.1029/2017GL076457>
- Teh, Y. A., Murphy, W. A., Berrio, J.-C., Boom, A., & Page, S. E. (2017). Seasonal variability in methane and nitrous oxide fluxes from tropical peatlands in the Western Amazon basin. *Biogeosciences*, 14(15), 3669–3683. <https://doi.org/10.5194/bg-14-3669-2017>
- Teh, Y. A., Silver, W. L., Conrad, M. E., Borglin, S. E., & Carlson, C. M. (2006). Carbon isotope fractionation by methane-oxidizing bacteria in tropical rain forest soils. *Journal of Geophysical Research*, 111(2), 1–8. <https://doi.org/10.1029/2005JG000053>
- Wanninkhof, R. (1992). Relationship between wind speed and gas exchange over the ocean. *Journal of Geophysical Research*, 97(C5), 7373–7382. <https://doi.org/10.1029/92JC00188>
- Warren, M., Hergoualc'h, K., Kauffman, J. B., Murdiyarso, D., & Kolka, R. (2017). An appraisal of Indonesia's immense peat carbon stock using national peatland maps: Uncertainties and potential losses from conversion. *Carbon Balance and Management*, 12(1), 12. <https://doi.org/10.1186/s13021-017-0080-2>
- Wong, G. X., Hirata, R., Hirano, T., Kiew, F., Aeries, E. B., Musin, K. K., et al. (2018). Micrometeorological measurement of methane flux above a tropical peat swamp forest. *Agricultural and Forest Meteorology*, 256–257, 353–361. <https://doi.org/10.1016/j.agrformet.2018.03.025>
- Wong, G. X., Hirata, R., Hirano, T., Kiew, F., Aeries, E. B., Musin, K. K., et al. (2020). How do land use practices affect methane emissions from tropical peat ecosystems? *Agricultural and Forest Meteorology*, 282–283, 107869. <https://doi.org/10.1016/j.agrformet.2019.107869>